Geometrical Grouplets

Stéphane Mallat
CMAP, Ecole Polytechnique, 91128 Palaiseau Cedex
To appear in Applied and Computational Harmonic Analysis, 2008

18 février 2008

Abstract

Grouplet orthogonal bases and tight frames are constructed with association fields that group points to take advantage of geometrical image regularities in space or time. These association fields have a multiscale geometry that can incorporate multiple junctions. A fast grouplet transform is computed with orthogonal multiscale hierarchical groupings. A grouplet transform applied to wavelet image coefficients defines an orthogonal basis or a tight frame of grouping bandlets. Applications to noise removal and image zooming are shown.

1 Geometric Image Processing

Geometry is at the heart of perception and is required to improve state of the art image processing algorithms. A drawing with few lines gives a powerful perception of shapes and textures. Motion fields provide geometrical information necessary for video processing. Understanding how to represent complex geometrical structures and derive sparse representations is a key issue for image processing. Recent neurophysiological experiments have lead to interesting new models.

The "Gestalt" psychophysic school gives a unifying theory of geometric perception through grouping processes. Neurophysiological studies have shown the existence of "neural integration" processes that may be responsible for these visual geometric groupings. This neural integration seems to first connect simple cells that implement a transformation similar to a wavelet transform in the V1 visual cortex. According to physiological models [16], a simple cell in V1 provides a wavelet coefficient at a given retina location, with a fixed scale and orientation selectivity that depends upon its position in a hypercolumnar structure [1]. These

cells also have non-linear behavior that have been interpreted as gain control feedback loops [11]. Experiments have shown the existence of "horizontal connections" that bind simple cells depending upon the image geometry [25]. The relation between horizontal connections and Gestalt grouping was done by Fields, Hayes and Hesse [8] with "pop out" experiments on images of Gabor patches. They model this horizontal connectivity through an association field between simple cells having a similar orientation selectivity. These association fields seem to be part of a hierarchical computational structure, with neurons in V2 integrating some geometric information provided by V1 simple cells, through feed-forward and feed-back connections. Some of these V2 neurons have been shown [16] to be sensitive to higher level geometrical structures such as the illusory contours of Kanizsa triangles [9]. Several ad-hoc models have been proposed [13] to explain the formation of association fields and the neuronal integration that is performed in V2, but physiological data are not precise enough to validate any precise model.

Wavelet transforms can adapt the processing resolution to the local image regularity but they cannot take advantage of geometrical directional regularity. From a mathematical point of view, building a hierarchical geometrical representation over wavelet coefficients is a natural idea because wavelet coefficients inherit the geometrical regularity of the image [15]. Several new bases have been elaborated to take advantage of the anisotropic regularity of geometrical image structures. Curvelets [3], contourlets [6], bandlets [14], wedgelets [7] are examples among others. Asymptotic results have been established for "cartoon-like" image models, defined as piecewise regular with edges along piecewise regular curves. For such images, these new bases provide more efficient asymptotic approximation, compression and denoising results than wavelet bases. Numerical improvements have also been demonstrated on real images. However, these improvements are not as spectacular as one may expect from the asymptotic theorems. This may be due to the relatively small portion of regular geometrical curves in real images, whereas textures often have a more complex geometry not efficiently represented by these bases.

For video compression and geometric image processing, more flexible directional multiscale decompositions have been developed with lifting schemes. A lifting is computed over embedded grids by associating each point to a neighbor point in a direction of maximum regularity. For video, the association field is derived from a computed motion between two images, and the lifting is calculated along a "motion threads" defined by the associations of pixels from one image to the next [23, 17]. In space, edge adaptive lifting schemes associate coefficients along the local orientation of edges, often calculated with a gradient operators [10, 12] or with block based optimisations [4]. Directional liftings have also been implemented over wavelet coefficients [5]. Adaptive directional lifting schemes satisfy perfect reconstruction properties, but they are not orthogonal and their stability is often

not controlled.

This paper introduces grouplet orthogonal bases and tight frames that build a stable geometrical image representation with an orthogonal weighted Haar lifting. In the spirit of the "Gestalt" psychophysic school, the geometry is constructed with grouping processes which define multiscale association fields. Grouplet orthogonal bases are constructed in Section 2 with these multiscale association fields. Section 2.2 describes more flexible grouplet tight frames that do not require embedded grid structures, with *causal* association fields. Noise removal and super-resolution image zooming algorithms are obtained by thresholding grouplet coefficients in Section 2.3. Section 3 introduces a hierarchical geometrical image representation by applying multiscale grouplet transforms over wavelet coefficients, which yields *grouping bandlet* orthogonal bases and tight frames. Applications are also described to remove noise from images and restore fine geometrical textures.

2 Multiscale Groupings with Association Fields

2.1 Orthogonal Grouplet Bases

An orthogonal multiscale grouping is implemented with a weighted Haar lifting applied successively to points that are grouped by an association field. The Haar transform is reviewed and then modified to define a grouplet transform.

Haar transform An average signal $a[n]$ is initially set to be equal to the input signal $f[n]$: $a[n] = f[n]$ for $0 \leq n < N$. Then, for a scale 2^j that increases from 2^1 to 2^J, and for all $0 \leq n < 2^{-j}N$, the Haar transform groups consecutive average coefficients $a[2n]$ and $a[2n+1]$, and it computes a next scale average

$$a[n] = \frac{a[2n] + a[2n+1]}{2} \ , \tag{1}$$

together with a normalized difference :

$$d_j[n] = (a[2n+1] - a[2n])\sqrt{2^{(j-1)}}. \tag{2}$$

The resulting coefficient $a[n]$ at a scale 2^j is the average of the signal values $f[p]$ for $p \in [2^j n, 2^j n + 2^j - 1]$ whereas the difference $d_j[n]$ is proportional to the difference between the averages of $f[p]$ on $[2^j n, 2^j n + 2^{j-1} - 1]$ and on $[2^j n + 2^{j-1}, 2^j n + 2^j - 1]$. At the largest scale 2^J, the average coefficients are renormalized $a_J[n] = 2^{J/2}\, a[n]$ to be an inner product between f and a vector of unit norm. The set of coefficients $\{d_j[n]\ ,\ a_J[n]\}_{1 \leq j \leq J, n}$ are inner products of f with vectors of a Haar orthonormal basis.

Association Fields on Embedded Grids An orthogonal grouplet transform modifies the Haar transform with an association field that groups together points that are not necessarily neighbors. Let us consider a multidimensional signal $f[n]$ defined over a multidimensional sampling grid $\mathcal{G}_0$. According to lifting transforms, a sequence of embedded subgrids $\{\mathcal{G}_i\}_{1\leq j\leq J}$ with $\mathcal{G}_{j+1}\subset\mathcal{G}_j$ is defined within $\mathcal{G}_0$. For each scale 2^j, following the lifting strategy, each $\mathcal{G}_j$ is divided into complementary subgrids $\mathcal{G}_{j+1}$ and $\tilde{\mathcal{G}}_{j+1}$ which are respectively called "average" and "difference"grids at the scale 2^{j+1}. These subgrids do not intersect and $\mathcal{G}_j = \mathcal{G}_{j+1}\cup\tilde{\mathcal{G}}_{j+1}$. The topology of "average" and "difference" subgrid decomposition of each average grid $\mathcal{G}_j$ can be freely chosen. Clearly all difference grids $\tilde{\mathcal{G}}_j$ are disjoint and

$$\mathcal{G}_0 = \cup_{j=1}^{J}\tilde{\mathcal{G}}_j \cup \mathcal{G}_J \ .$$

Each $\tilde{m}\in\tilde{\mathcal{G}}_j$ will be grouped with a point $m\in\mathcal{G}_j$ such that the neighborhood values of $a[\tilde{m}]$ "are similar" to the neighborhood values of $a[m]$. The difference of positions is stored in an association field array : $A_j[\tilde{m}] = m-\tilde{m}$. Since the grids $\mathcal{G}_j$ are embedded, when the scale 2^j increases the distance between samples of these grids increases. The association fields A_j thus group points whose distance increase with the scale 2^j.

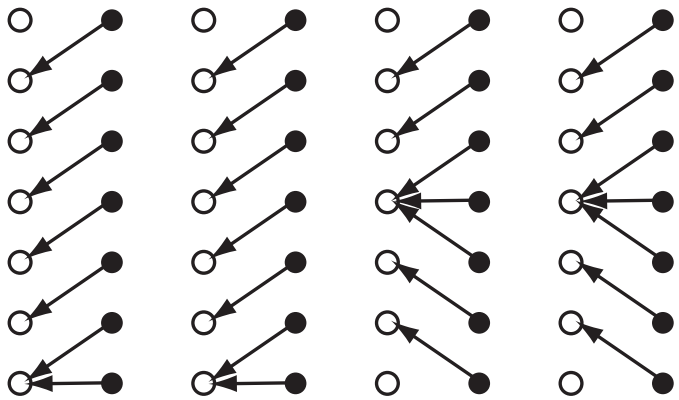

FIG. 1 – *Column embedded grids subsample the columns of $\mathcal{G}_{j-1}$ to define the grid $\mathcal{G}_j$ (white points) and the complementary grid $\tilde{\mathcal{G}}_j$ (black points). The association field groupings are illustrated by arrows.*

The topology of the subgrids $\mathcal{G}_j$ can be adapted to the image geometrical regularity and may even vary depending upon the scale 2^j. If the image geometrical structures are elongated along a preferential direction, then one can subsample $\mathcal{G}_j$ along the perpendicular direction. For example, seismic images such as Fig. 3 have a layered structure that is rather horizontal. The grouping should thus relate points are not in the same column. To implement such groupings, $\mathcal{G}_j$ is decomposed into its even columns corresponding to $\mathcal{G}_{j+1}$ and its odd columns corresponding to

$\tilde{\mathcal{G}}_{j+1}$. This defines *column embedded subgrids*. Fig. 1 illustrates an association field defined with column embedded subgrids. If the image has geometrically regular structures that rather propagate vertically, then $\mathcal{G}_j$ is decomposed into even and odd rows corresponding respectively to $\mathcal{G}_{j+1}$ and $\tilde{\mathcal{G}}_{j+1}$. This defines *rows embedded subgrids*. When the image has no preferential direction, one may choose more isotropic subgrids, such as quincunx subgrids.

Although this paper mostly concentrates on geometrical structures of two-dimensional images, association fields and their corresponding grouplet bases may be defined in any dimension. For videos, $\mathcal{G}_0$ is a three dimensional grid which is a time sequence of two-dimensional image sampling grids. At each scale 2^j, time embedded subgrids can decompose $\mathcal{G}_j$ into even time images $\mathcal{G}_{j+1}$ and odd time images $\tilde{\mathcal{G}}_{j+1}$. An association field $A_j[\tilde{m}]$ typically stores a time displacement from $\tilde{m} \in \tilde{\mathcal{G}}_j$ to the previous image point $m \in \mathcal{G}_j$. Other space-time subsampling grids may be chosen to potentially take advantage simultaneously of spatial and time geometric regularities. However, in more than two dimensions, no embedded subgrid scheme characterized by a subsampling matrix with reduction factor 2 can have an isotropic behavior similar to a two-dimensional quincunx grid [24].

Orthogonal Grouplets A grouplet transform is a weighted multiscale Haar transform. The average signal is also initialized to be the input signal $a[n] = f[n]$ for all $n \in \mathcal{G}_0$. A new array $s[n]$ is created to store the support size of the averaging kernel which computes $a[n]$ from f. At the initialization, since $a[n] = f[n]$ it results that $s[n] = 1$.

For scales 2^j that increase from 1 to 2^J, the successive groupings are performed in a predefined order over all points in $\tilde{\mathcal{G}}_j$. Let N_j be the number of samples of $\tilde{\mathcal{G}}_j$. Let α_j be an invertible mapping between $1 \leq n \leq N_j$ and points $\tilde{m} = \alpha_j(n) \in \tilde{\mathcal{G}}_j$. For n going from 1 to N_j, each $\tilde{m} = \alpha_j(n)$ is associated to a point $m = \tilde{m} + A_j[\tilde{m}]$. The grouplet transform computes a normalized difference between associated averages :

$$d_j[\tilde{m}] = \Big(a[\tilde{m}] - a[m]\Big) \frac{\sqrt{s[m]\, s[\tilde{m}]}}{\sqrt{s[m] + s[\tilde{m}]}} \,. \tag{3}$$

The new weighted average is

$$\widehat{a} = \frac{s[m]\, a[m] + s[\tilde{m}]\, a[\tilde{m}]}{s[m] + s[\tilde{m}]}, \tag{4}$$

and the averaging size is updated by adding the averaging size of the two averaged points

$$\widehat{s} = s[m] + s[\tilde{m}]. \tag{5}$$

These values are stored "in place" at $m \in \mathcal{G}_j$: $a[m] = \widehat{a}$ and $s[m] = \widehat{s}$.

The flexibility of the grouping process can take advantage of various geometric regularity including periodic patterns and junctions. At junction points, several points may be grouped with a single one, with successive orthogonalizations, as illustrated by Fig. 1.

At the largest scale $2^j = 2^J$, average coefficients are normalized by setting

$$\forall m \in \mathcal{G}_J \quad , \quad a_J[m] = a[m] \sqrt{s[m]} \ . \tag{6}$$

The grouplet transform associates to a signal $f[n]$ of size N the family of N grouplet coefficients $\{d_j[\tilde{m}] \ , \ a[m]\}_{1 \leq j \leq J, \tilde{m} \in \tilde{\mathcal{G}}_j, m \in \mathcal{G}_J}$. The grouplet representation includes not only these coefficients but also the $N(1 - 2^{-J})$ multiscale association field coefficients $\left\{A_j[\tilde{m}]\right\}_{1 \leq j \leq J, \tilde{m} \in \tilde{\mathcal{G}}_j}$. For each $\tilde{m} \in \mathcal{G}_j$, (3), (4) and (5) is computed with $O(1)$ operations. Like in a Haar transform, the N grouplet coefficients are thus computed with $O(N)$ operations. The overall numerical complexity will be dominated by the number of operations required to compute the $N(1 - 2^{-J})$ association field coefficients which is typically larger.

Since a grouplet transform is linear, each difference coefficient can be written as an inner product of $f[n]$ with a difference grouplet vector $g_{j,\tilde{m}}[n]$:

$$d_j[\tilde{m}] = \langle f \ , \ g_{j,\tilde{m}} \rangle = \sum_n f[n] \, g_{j,\tilde{m}}[n]. \tag{7}$$

At the coarsest scale, each normalized average coefficient is also an inner product with an average grouplet vector $h_{J,m}[n]$:

$$a_J[m] = \langle f \ , \ h_{J,m} \rangle \ . \tag{8}$$

The following theorem proves that average and difference grouplet vectors have properties similar to Haar vectors.

Theorem 2.1.
- *(i) For any $m \in \mathcal{G}_J$, $h_{J,m}[n] = 1/\sqrt{s[m]}$ over its support whose size is $s[m]$.*
- *(ii) For any scale 2^j and $\tilde{m} \in \tilde{\mathcal{G}}_j$, $g_{j,\tilde{m}}[n]$ has 1 vanishing moment and takes only two different values over its support.*

Proof. A grouplet transform is implemented by iterating a cascade of elementary operators specified by (3), (4) and (5). After applying k such unitary operators in the order defined by the algorithm, each $a[m]$ is the result of a linear operator applied to $f[n]$ and hence can be written $a[m] = \langle \tilde{h}_{k,m}[n], f[n] \rangle$. Let $m = \tilde{m} + A_j[\tilde{m}] \in \mathcal{G}_{j+1}$ be the point grouped with $\tilde{m} \in \tilde{\mathcal{G}}_{j+1}$ by the $k+1$ unitary operator. As a result of (4) we have

$$\tilde{h}_{k+1,m}[n] = \frac{s[m] \, \tilde{h}_{k,m}[n] + s[\tilde{m}] \, \tilde{h}_{k,\tilde{m}}[n]}{s[m] + s[\tilde{m}]}. \tag{9}$$

Let us first prove that the supports of $\tilde{h}_{k,m}[n]$ and $\tilde{h}_{k,\tilde{m}}[n]$ do not intersect. Observe that the support of $\tilde{h}_{k,m}$ is the union of all points aggregated by the association fields A_l for $l \leq j$. This grouping defines a tree over the support of $\tilde{h}_{k,m}$ whose root is m. Indeed, an association field A_l groups a point in $\tilde{\mathcal{G}}_l$ to a point in $\mathcal{G}_l$ which thus belongs to a grid $\tilde{\mathcal{G}}_k$ for some $k > l$ or to $\mathcal{G}_J$. Since the grouping goes from a finer to a larger scale grid, there cannot be any cycle and the root is the point m at the largest scale.

Similarly the support of $\tilde{h}_{k,\tilde{m}}$ has a tree structure rooted at $\tilde{m}$. We also know that $\tilde{m}$ and m do not belong to the support respectively of $\tilde{h}_{k,m}$ and $\tilde{h}_{k,\tilde{m}}$. Indeed, m cannot belong to the support of $\tilde{h}_{k,\tilde{m}}$ since m is in a coarser grid than $\tilde{m}$, and $\tilde{m}$ cannot belong to the support of $\tilde{h}_{k,m}$ because $\tilde{m}$ has not yet been grouped to a coarser scale point by the aggregation process.

Since the supports of $\tilde{h}_{k,m}$ and $\tilde{h}_{k,\tilde{m}}$ are trees and none of their roots belong to the other tree, necessarily these trees are disjoint which means that these supports do not intersect.

Let us now prove by induction on k that $\tilde{h}_{k,m}[n] = 1/s[m]$ over a support of size $s[m]$. For $k = 0$ this property is valid since $\tilde{h}_{0,m}[n] = \delta[n-m]$ and $s[m] = 1$. Suppose that the induction hypothesis is valid for k. It implies that $\tilde{h}_{k,m} = 1/s[m]$ and $\tilde{h}_{k,\tilde{m}} = 1/s[\tilde{m}]$ over their support of size respectively $s[m]$ and $s[\tilde{m}]$. Since $\tilde{h}_{k,m}$ and $\tilde{h}_{k,\tilde{m}}$ have disjoint supports, it results from (9) that $\tilde{h}_{k+1,m} = 1/(s[m] + s[\tilde{m}])$ over its support of size $s[m] + s[\tilde{m}]$. The updating formula (5) with $s[m] = \widehat{s}$ thus verifies that the induction hypothesis is valid for $k+1$. Incorporating the normalization (6) at the coarsest scale finishes the proof of (i).

To prove (ii), as a result of (3) we can write

$$g_{j,\tilde{m}} = (\tilde{h}_{k,\tilde{m}} - \tilde{h}_{k,m}) \frac{\sqrt{s[m]s[\tilde{m}]}}{\sqrt{s[m] + s[\tilde{m}]}} \ . \tag{10}$$

Since $h_{k,\tilde{m}} = 1/s[\tilde{m}]$ and $h_{k,m} = 1/s[m]$ over their support of size respectively $s[\tilde{m}]$ and $s[m]$, and their support are disjoint, it results that $g_{j,\tilde{m}}$ takes only two different values over its support. Moreover we verify that $\sum_n g_{j,\tilde{m}}[n] = 0$ and hence that $g_{j,\tilde{m}}$ has 1 vanishing moment. □

Theorem 2.1 proves that the support of grouplet vectors have a tree structure with a support size equal to $s[m]$. Junctions correspond to points where grouplet supports have several "sons" defined by multiple groupings with a single junction point. The following theorem proves that grouplets define an orthonormal basis.

Theorem 2.2. *The grouplet family*

$$\left\{ g_{j,\tilde{m}}[n] \ , \ h_{J,m}[n] \right\}_{1 \leq j \leq J, \tilde{m} \in \mathcal{G}_j, m \in \mathcal{G}_J}$$

is an orthonormal basis of $\mathbf{l^2}(\mathcal{G}_0)$.

Proof.

Lemma 2.1. *For any $a, \tilde{a}, s > 0$ and $\tilde{s} > 0$, we define*

$$\widehat{s} = s + \tilde{s} \quad , \quad d = (a - \tilde{a})\frac{\sqrt{s\tilde{s}}}{\sqrt{\widehat{s}}} \quad \text{and} \quad \widehat{a} = \frac{s\,a + \tilde{s}\,\tilde{a}}{\widehat{s}}. \tag{11}$$

The operator that transforms $(a\sqrt{s}\,,\,\tilde{a}\sqrt{\tilde{s}})$ into $(d\,,\,\widehat{a}\sqrt{\widehat{s}})$ is a unitary operator.

This lemma is proved by observing that the two rows of the 2×2 matrix of this operator are $(\sqrt{\tilde{s}}\,,\sqrt{s})/\sqrt{s+\tilde{s}}$ and $(\sqrt{s}, -\sqrt{\tilde{s}})/\sqrt{s+\tilde{s}}$, which are two orthonormal vectors. It is therefore a unitary operator.

Lemma 2.1 proves that the operator which transforms $(a[m]\,\sqrt{s[m]}\,, a[\tilde{m}]\sqrt{s[\tilde{m}]})$ into $(\widehat{a}\,\sqrt{\widehat{s}}, d_j[\tilde{m}])$ as defined by (3), (4) and (5) is a unitary operator. Let $a_j[m] = a[m]\sqrt{s[m]}$ be the normalized average array at the end of the loop over the index n that goes from 1 to N_j, for a given j. The operator which transforms $\{a_{j-1}[m]\}_{m\in\mathcal{G}_{j-1}}$ into $\{a_j[m], d_j[\tilde{m}]\}_{m\in\mathcal{G}_j,\tilde{m}\in\tilde{\mathcal{G}}_j}$ is therefore a cascade of N_j unitary operators and is thus a unitary operator. At the initialization $a_0[m] = a[m]\sqrt{s[m]} = f[m]$ for all $m \in \mathcal{G}_0$. It results that iterating over the variable j defines a cascade of unitary operators that transforms $f[m]$ in to the grouplet coefficients

$$\Big\{d_j[\tilde{m}]\ ,\ a_J[m]\Big\}_{1\le j\le J,\tilde{m}\in\tilde{\mathcal{G}}_j,m\in\mathcal{G}_J}\ .$$

As a consequence, the grouplet vectors defined by (7) and (8) define an orthonormal basis. □

Inverse Orthogonal Grouplet Transform Since grouplets define an orthonormal basis, the input signal can be reconstructed from its grouplet coefficients with :

$$f[n] = \sum_{j=1}^{J}\sum_{\tilde{m}\in\mathcal{G}_j} d_j[\tilde{m}]\,g_{j,\tilde{m}}[n] + \sum_{m\in\mathcal{G}_J} a_J[m]\,h_{J,m}[n]\ . \tag{12}$$

Similarly to the fast inverse Haar transform, the fast inverse grouplet transform inverts each grouping operator in the reverse order of the forward transform, for a scale 2^j that decreases from 2^J to 1.

The averaging size array is recalculated at the coarsest scale 2^J from the association fields. We initialize $s[m] = 1$ for all $m \in \mathcal{G}_0$ and for j going from 1 to J and for all $\tilde{m} \in \tilde{\mathcal{G}}_j$

$$\widehat{s} = s[m] + s[\tilde{m}] \quad \text{and} \quad s[m] = \widehat{s} \quad \text{for} \quad m = \tilde{m} + A_j[\tilde{m}]\ .$$

At the coarsest scale, 2^J, the average coefficient normalization (6) is then inverted

$$\forall m \in \mathcal{G}_J \quad , \quad a[m] = \frac{a_J[m]}{\sqrt{s[m]}} \ . \tag{13}$$

Each grouping transform is then inverted at each scale in their reverse order. For j going from J to 1 and for n going from N_j to 1 let $\tilde{m} = \alpha_j(n)$ and $m = \tilde{m} + A_j[\tilde{m}]$. To invert the grouping transform, the averaging size is updated by inverting (5)

$$\tilde{s} = s[m] - s[\tilde{m}] \tag{14}$$

and the finer scale average coefficients are computed from the larger scale average coefficient and the difference coefficient by inverting the unitary transform defined by (3) and (4) :

$$a[\tilde{m}] = a[m] + d_j[\tilde{m}] \, \frac{\sqrt{\tilde{s}}}{\sqrt{s[\tilde{m}] \, s[m]}} \tag{15}$$

$$\tilde{a} = a[m] - d_j[\tilde{m}] \, \frac{\sqrt{s[\tilde{m}]}}{\sqrt{\tilde{s} \, s[m]}} \ . \tag{16}$$

These reconstructed values are stored "in place" $a[m] = \tilde{a}$ and $s[m] = \tilde{s}$. At the end of this double loop over all groupings at all scales, this inversion reconstructs the original signal $a[m] = f[m]$ for all $m \in \mathcal{G}_0$.

For each $\tilde{m} \in \mathcal{G}_j$ the reconstruction operations (14), (15) and (16) requires $O(1)$ operations. The N signal coefficients $f[m]$ are thus recovered with $O(N)$ operations.

Multiscale Association Fields and Best Basis There are as many grouplet orthonormal bases as possible groupings of signal samples. Computing multiscale association fields is thus equivalent to choose a "best" grouplet basis to decompose a particular image. The representation does not only include the grouplet coefficients $d_j[m]$ but also the association fields $A_j[m]$. For image compression applications, it is necessary to code both the grouplet coefficients and the association fields, with as few bits as possible. Few bits are needed to encode the difference coefficients $d_j[\tilde{m}]$ if few of these coefficients are non-zero after quantization. This means that each $\tilde{m} \in \tilde{\mathcal{G}}_j$ should be associated to a point $m = \tilde{m} + A_j[\tilde{m}]$ such that $|a[m] - a[\tilde{m}]|$ is small. The ability to code efficiently an association field depends upon its regularity. If it is highly regular then it can be approximated with few coefficients that can be encoded for example in a wavelet or polynomial spline basis. We thus need to compute regular association fields that produce sparse grouplet coefficient sequences.

Grouplet orthonoral bases have a flexible geometry but the resulting dictionary is more complex than the "tree-structured" dictionaries used for wedglets [7]

or bandlets [14]. As a consequence, optimizing the multiscale association fields to minimize the distortion-rate of a grouplet signal compression is a more complex problem, that is beyond the scope of this paper. A finer mathematical analysis of grouplet dictionary properties for video processing can be found in [19]. We describe below a simple block matching algorithm that is used in numerical experiments.

Block matching algorithms are often used to compute displacements, for motion estimation in video. For each $\tilde{m} \in \tilde{\mathcal{G}}_j$, the search for a best match is performed in a neighborhood of $\tilde{m}$ of points in $\mathcal{G}_j$, that we write $\mathcal{N}_j(\tilde{m})$. A block matching computes for all $p \in \mathcal{N}_j(\tilde{m})$ the $\mathbf{l^1}$ or $\mathbf{l^2}$ distance between a block of points $B(p)$ of $\mathcal{G}_j$ around p and the corresponding block around $\tilde{m}$, and it finds the $p = m$ which minimizes this distance :

$$m = \text{argmin}_{p \in \mathcal{N}_j(\tilde{m})} \sum_{n \in B(p)} \left| a[n] - a[n + \tilde{m} - p] \right|^k \quad \text{with } k = 1 \text{ or } k = 2. \tag{17}$$

If each block $B(p)$ has P points and the size of each neighborhood $\mathcal{N}_j(\tilde{m})$ has K points then for a signal of size N this block matching requires $O(K\,P\,N)$ operations to compute all association field coefficients. It is typically much larger than the $O(N)$ operations needed to compute the resulting grouplet coefficients.

When increasing the size P of $B(p)$, the regularity of the association field increases. However, the center point p becomes relatively less important in the distance minimization, which typically increases the resulting best match difference $|a[m] - a[\tilde{m}]|$. Reducing the size K of the neighborhood $\mathcal{N}_j(\tilde{m})$ reduces the range of values of the association fields, but reducing the possible associations may also increase the best match difference $|a[m] - a[\tilde{m}]|$. The choice of a block size and a neighborhood size search is thus a trade-off between the sparsity of the grouplet coefficients and the regularity or complexity of the multiscale association fields.

In the example of seismic images, $\mathcal{G}_j$ is obtained by subsampling by a factor 2^j the image columns. For each $\tilde{m} \in \tilde{\mathcal{G}}_j$, finding its best match amounts to finding the orientation of the layer that goes through $\tilde{m}$. The neighborhood search $\mathcal{N}_j(\tilde{m})$ must thus correspond to enough possible orientations to choose an appropriate one. One can restrict $\mathcal{N}_j(\tilde{m})$ to an interval of points in the previous column of $\mathcal{G}_j$, centered on the same row as $\tilde{m}$, as illustrated in Fig. 2(a). The size of this interval is typically proportional to 2^j to provide a sufficiently wide angle range that is independent of the scale. The neighborhood $\mathcal{N}_j(\tilde{m})$ can also be extended beyond the previous column and cover a set points of $\mathcal{G}_j$ whose positions with respect to $\tilde{m}$ provides a sufficiently fine sampling of all possible orientations, as illustrated in Fig. 2(b).

Fig. 3 shows the multiscale association fields computed with a block matching with a neighborhood search restricted to the previous column, as in Fig. 2(a). The

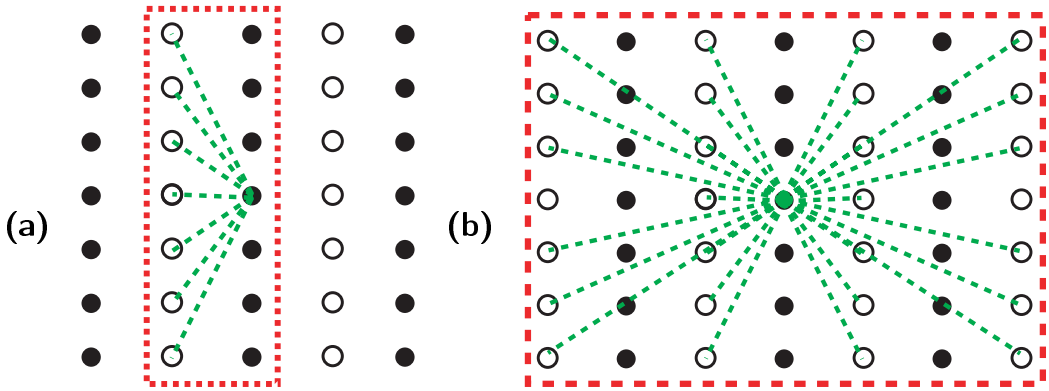

FIG. 2 – *Possible matches for $\tilde{m} \in \tilde{\mathcal{G}}_j$ in a neighborhood $\mathcal{N}_j(\tilde{m}) \subset \mathcal{G}_j$ that is an interval in the previous column in (a) and a wider set of points covering more directions in (b).*

block matching computes regular multiscale association fields with directions along which the image is smoothly varying.

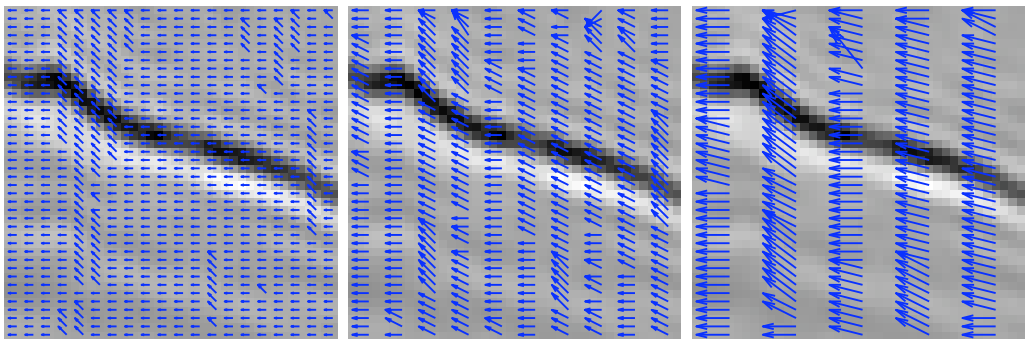

FIG. 3 – *Grouping of an association field at scales 2^1, 2^2 and 2^3 computed by block matching for a seismic image shown in transparency.*

Fig. 4(b) shows orthogonal grouplet coefficients over $J = 6$ scales, computed from the multiscale association fields displayed in Fig. 3. Black, gray and white coefficients correspond to negative, zero and positive coefficients with the same dynamic range as in the original seismic image in Fig. 4(a). There are mostly gray coefficients which means that most "difference" coefficients of the multiscale grouping orthogonal transform are nearly zero. Fig. 4(c) shows example of grouplet vectors $g_{j,m}[n]$ for several scales 2^j. These grouplet vectors have a support which is elongated along the association field, with possible junctions and a tree structure. Fig. 4(d) gives another example of orthogonal grouplet coefficients computed on Lena's hat, with $J = 6$ scales. The grouplet representation is clearly much more

sparse than the original image.

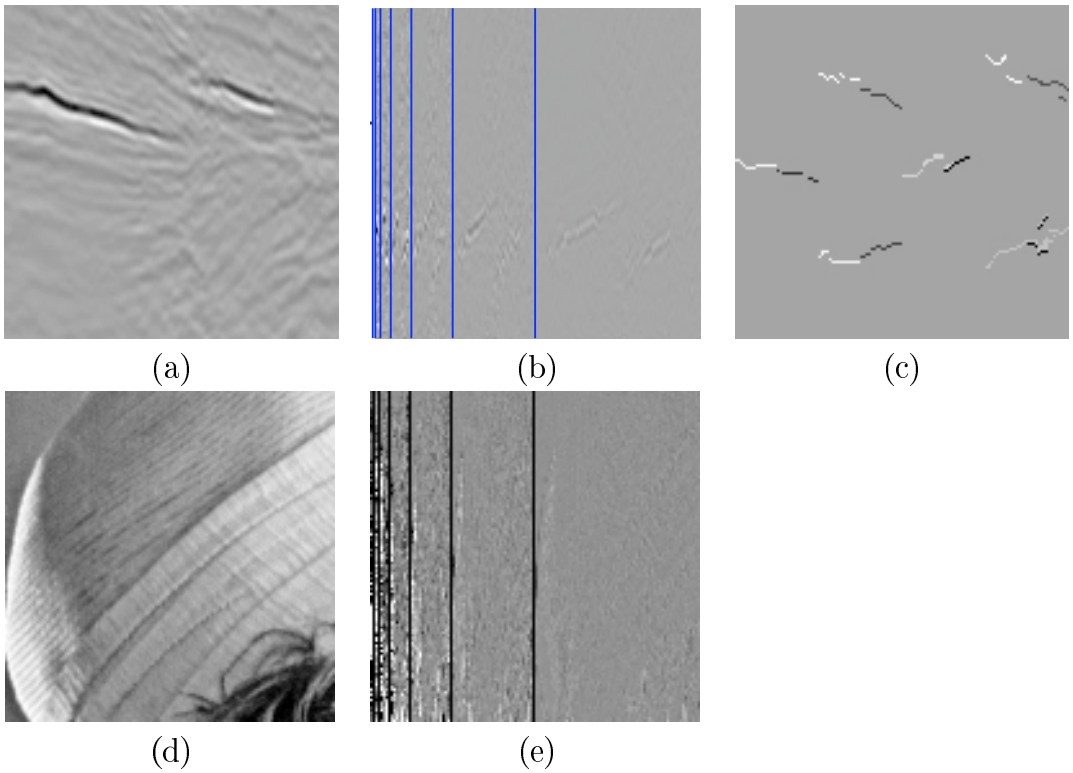

FIG. 4 – *(a,d) : Original images. (b,e) : Orthogonal grouplet coefficients over 6 scales, displayed with the same dynamic range as the original image. (c) Examples of grouplet vectors* $g_{j,\tilde{m}}$.

Matching Pursuit If the multiscale association field $A_j[\tilde{m}]$ is computed together with the grouplet decomposition the resulting algorithm is similar to an orthogonal matching pursuit. In the algorithm previously described, for each scale 2^j, the iteration begins by a computation of the association field $A_j[\tilde{m}]$ for all $\tilde{m} \in \tilde{\mathcal{G}}_j$ followed by a computation of all difference coefficients $d_j[\tilde{m}]$ for all $\tilde{m} \in \tilde{\mathcal{G}}_j$. A second possibility is to compute for each $\tilde{m} = \alpha_j(n)$ the value of $A_j[\tilde{m}]$, then calculate $d_j[\tilde{m}]$ and update $a[m]$ for $m = \tilde{m} + A_j[\tilde{m}]$, before computing the next association field value for $\tilde{=}\alpha_j(n+1)$. This reordering of calculations does not change the overall computational complexity. This calculation is similar to a *matching pursuit* decomposition [20] where each vector is sequentially computed by a greedy optimization which finds a best match. In this case, the pursuit is orthogonal with no further orthogonalization required. It is computed in a fine to coarse order, with fine scale vectors first and coarse scale vectors afterward. This

pursuit is performed in the dictionary of all possible grouplets corresponding to all possible association fields.

2.2 Grouplet Tight Frames

Redundant grouplet tight frames can be constructed without an embedded subgrid structure. More flexible multiscale association fields are defined with a causality property which is sufficient to construct grouplets having an energy conservation as in the orthogonal case. These association fields have more flexibility as in the models [8] of Fields, Hayes and Hesse [8] for horizontal connections between simple cells in the visual cortex region V1. The redundancy of these grouplet tight frames also improves noise removal with thresholding estimators.

Causal Multiscale Association Fields To avoid grouping a point $\tilde{m}$ with m and then group m with $\tilde{m}$, a causality is imposed on the association field, with a partial ordering of all points in the signal sampling grid $\mathcal{G}_0$. An association field A_j is said to be *causal* if it groups each $\tilde{m} \in \mathcal{G}_0$ with a point $m = \tilde{m} + A_j[\tilde{m}] \in \mathcal{G}_0$ that is located *before* $\tilde{m}$ in the sense of this partial ordering. If there is no point *before* $\tilde{m}$ then we set $A_j[\tilde{m}] = \text{NULL}$.

A causal multiscale association field must also associate points whose distance increase with the scale 2^j, to reach long range groupings for large scales. For a given pseudo distance $d(x, y)$ defined over points in $\mathbb{R}^2$, we impose that for any scale 2^j if $\tilde{m} + A_j[\tilde{m}] = m$ then $2^{j-1} \leq d(m, \tilde{m}) < 2^j$. A pseudo distance satisfies the symmetry and triangular inequality of a distance but one can have $d(x, y) = 0$ with $x \neq y$. We say that a causal association field is *strictly multiscale* if for any scale 2^j and any $m = A_j[\tilde{m}]$ we have $d(m, \tilde{m}) = 2^{j-1}$.

The partial ordering and the pseudo distance can be adapted to the type of geometrical regularity that must be captured by the grouping. For motion in a video frame sequence, at each scale 2^j a time causal strictly multiscale association field can associate an image point $\tilde{m}$ to a point m located in a previous image at distance of 2^{j-1} frames before. This association can be interpreted as a displacement over 2^{j-1} time steps. In this case, the partial ordering of image points is defined by the corresponding time frame location and the pseudo distance by the number of time steps between frames.

For spatial geometric grouping, a grouplet partial ordering can be defined with respect to a preferential direction of angle θ. A point $x = (x_1, x_2) \in \mathbb{R}^2$ is said to be before $\tilde{x} = (\tilde{x}_1, \tilde{x}_2) \in \mathbb{R}^2$ with respect to a partial ordering of angle θ if

$$x_1 \cos\theta + x_2 \sin\theta < \tilde{x}_1 \cos\theta + \tilde{x}_2 \sin\theta. \tag{18}$$

This type of ordering constructs grouplets whose support are elongated in the direction of θ as opposed to its perpendicular direction. It is particularly well

adapted to perform a grouplet transform of wavelet coefficients calculated with a wavelet having an orientation selectivity around $\theta + \pi/2$ as we shall see in Section 3.2. One can choose a causal pseudo-distance of angle θ defined by

$$d_\theta(x, y) = |x_1 \cos\theta + x_2 \sin\theta - y_1 \cos\theta - y_2 \sin\theta|$$

which is the distance of the projection of x and y on the line of angle θ going through $(0, 0)$. One can also use a Euclidean distance.

Other grouplet partial ordering may be defined from a distance to a center point $c = (c_1, c_2) \in \mathbb{R}^2$. A point $x = (x_1, x_2) \in \mathbb{R}^2$ is before $\tilde{x} = (\tilde{x}_1, \tilde{x}_2) \in \mathbb{R}^2$ with respect to c if

$$(x_1 - c_1)^2 + (x_2 - c_2)^2 < (\tilde{x}_1 - c_1)^2 + (\tilde{x}_2 - c_2)^2 \ . \tag{19}$$

This partial ordering is natural when there exists a singular point that plays a particular role. This is the case in the retina where the density of photoreceptors increases as a function of the distance to the fovea.

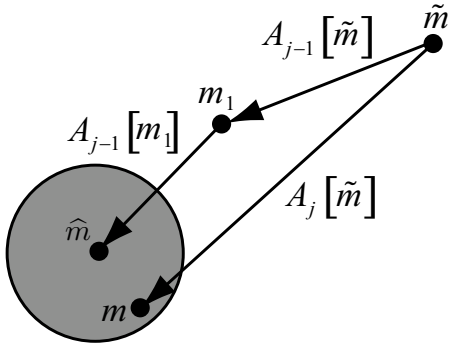

FIG. 5 – *An association field A_j is computed by propagating A_{j-1} over two points and by performing a local optimization.*

Many procedures may be used to compute causal association fields. The following algorithm guides the computation of large scale association fields from finer scale association fields, to reduce the numerical complexity. At a scale 2^j, for each $\tilde{m} \in \mathcal{G}_0$ the associated point $m \in \mathcal{G}_0$ is computed by propagating the association field at the finer scale 2^{j-1} over two points, and then by performing a local block matching optimization. The propagation of A_{j-1} over two points from $\tilde{m}$ yields

$$\widehat{m} = \tilde{m}_1 + A_{j-1}[\tilde{m}_1] \quad \text{with} \quad \tilde{m}_1 = \tilde{m} + A_{j-1}[\tilde{m}] \ .$$

Let $\mathcal{N}(\widehat{m})$ be neighborhood of $\widehat{m}$ in $\mathcal{G}_0$. A block matching computes for all $p \in \mathcal{N}(\widehat{m})$ located before $\tilde{m}$ the distance between a block of P points $B(p)$ of $\mathcal{G}_0$ around

p and the corresponding block around $\tilde{m}$, and it finds the $p = m$ which minimizes this distance :

$$m = \text{argmin}_{\substack{p \in \mathcal{N}(\tilde{m}) \\ p \text{ before } \tilde{m}}} \sum_{n \in B(p)} \Big| a[n] - a[n + \tilde{m} - p] \Big|^k \quad \text{with } k = 1 \text{ or } k = 2. \tag{20}$$

We set $A_j[\tilde{m}] = m - \tilde{m}$. This process is illustrated by Fig. 5. The association field A_j is thus derived from A_{j-1} plus an adjustment whose amplitude depends upon the size K of the neighborhoods $\mathcal{N}(\widehat{m})$, which is typically small. This adjustment is necessary to avoid accumulations of errors when following long range geometric structures. To compute the finest scale association field A_1, we initialize $A_0[\tilde{m}] = 0$ for all $\tilde{m} \in \mathcal{G}_0$. For a signal of size N, this block matching compute the $J\,N$ values of the J association fields A_j with $O(J\,N\,K\,P)$ operations. If the multiscale association field adjustment is suppressed then all association fields are derived from the finest scale association field A_1 and the computational complexity becomes $O(N\,K\,P + J\,N)$.

Fig. 6 shows a strictly multiscale causal association field over two scales calculated on a zoom of Lena's hat. A partial ordering of angle $\theta = 0$ is used, which means that coefficients are ordered columns by columns. A pseudo distance of angle $\theta = 0$, measuring the horizontal distance, is used by the grouping. At a scale 2^j, the grouping is performed between points whose columns have a distance of 2^{j-1}.

Tight Frame Grouplet Transform A grouplet frame transforms a signal $f[n]$ into multiscale difference coefficients and coarse scale average coefficients defined on the original signal grid $\mathcal{G}_0$. Similarly to orthogonal grouplet coefficients, these coefficients are computed with successive grouping transformations according to multiscale association fields. All points of $\mathcal{G}_0$ are visited in an order coherent with the grouplet partial ordering.

Suppose that $\mathcal{G}_0$ includes N samples. One can define an ordering function $\alpha(n)$ that is compatible with the grouplet partial ordering. It is an invertible mapping that associates to any integer $1 \leq n \leq N$ a point $\alpha(n) \in \mathcal{G}_0$ such that if $m = \alpha(n)$ is *before* $p = \alpha(u)$ with respect to the grouplet partial ordering, then $n < u$.

In a video time sequence, for a time partial ordering an ordering function sorts all image pixels in the time order, and within each image the pixels can be sorted in any spatial order. In a rectangular image with M_1 columns and M_2 rows, for a partial ordering of angle 0 (horizontal), an ordering function can be defined by $(m_1, m_2) = \alpha(m_2 + m_1 M_2)$, and for a partial ordering of angle $\pi/2$ (vertical) the ordering function can be $(m_1, m_2) = \alpha(m_1 + m_2 M_1)$.

For $j = 0$ and all $m \in \mathcal{G}_0$, the grouplet frame transform initializes $a[m] = f[m]$ with an averaging size $s[m] = 1$. For j going from 1 to J, and for all n going from

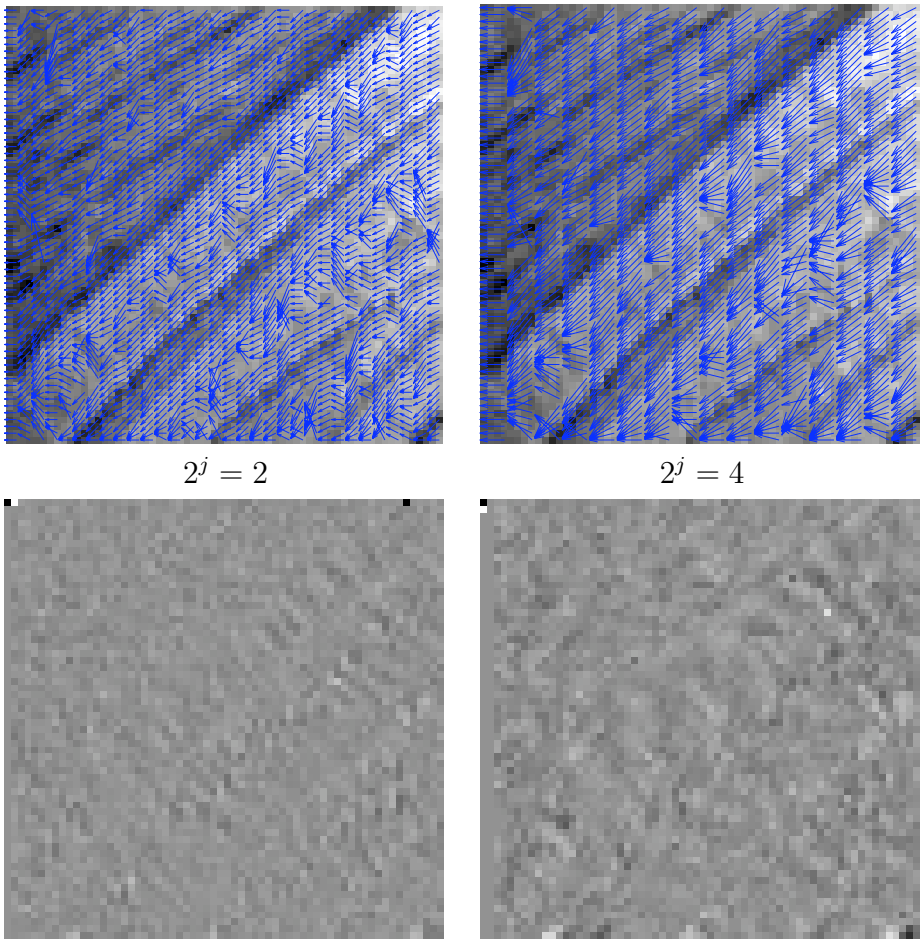

FIG. 6 – *Left and right columns display strictly multiscale causal association fields and the corresponding tight frame grouplet coefficients, at scales* 2^1 *and* 2^2*. Coefficients are shown on the same dynamic range as the original image.*

1 to N, let $\tilde{m} = \alpha(n)$. If $A_j[\tilde{m}] \neq$ NULL then for $m = \tilde{m} + A_j[\tilde{m}]$ the grouping defines a new averaging size

$$\widehat{s} = s[m] + s[\tilde{m}] \ , \tag{21}$$

a difference coefficient

$$d_j[\tilde{m}] = (a[\tilde{m}] - a[m]) \frac{\sqrt{s[m]s[\tilde{m}]}}{\sqrt{\widehat{s}}} \ , \tag{22}$$

and a new weighted average

$$\widehat{a} = \frac{s[m]\, a[m] + s[\tilde{m}]\, a[\tilde{m}]}{\widehat{s}}. \tag{23}$$

These values are stored "in place" : $a[m] = \widehat{a}$ and $s[m] = \widehat{s}$. If $A_j[\tilde{m}] = \text{NULL}$ then we perform a transform as if the associated point was 0 and set $d_j[\tilde{m}] = a[\tilde{m}]\sqrt{s[\tilde{m}]}$.

At the coarsest scale 2^J, as in the orthogonal grouplet transform, the average coefficients are normalized

$$\forall m \in \mathcal{G}_0 \quad , \quad a_J[m] = a[m]\,\sqrt{s[m]}\;. \tag{24}$$

A redundant grouplet transform is thus an operator G that associates to a signal $f[n]$ of size N a family of $J+1$ grouplet coefficient arrays $\left\{d_j[m], a_J[m]\right\}_{1\le j\le J, m\in\mathcal{G}_0}$ together with J multi-scale association field arrays $\{A_j[m]\}_{1\le j\le J, m\in\mathcal{G}_0}$. For a signal of size N, (21), (22) and (23) compute the $(J+1)\,N$ grouplet coefficients with $O(N\,J)$ operations.

Fig. 6 shows the grouplet tight frame coefficients of a textured image computed from a multiscale association field at scales 2^1 and 2^2. Most multiscale difference coefficients have a much smaller dynamic range than the original image coefficients.

Each $d_j[m]$ and $a_J[m]$, for $1 \le j \le J$ and $m \in \mathcal{G}_0$, is calculated with a linear operator and can thus be written as an inner product with a grouplet vector :

$$d_j[m] = \langle f, g_{j,m}\rangle \;\text{ and }\; a_J[m] = \langle f, h_{J,m}\rangle\;.$$

The family of grouplets $\{g_{j,m}\}_{1\le j\le J, m\in\mathcal{G}_0} \cup \{h_{J,m}\}_{m\in\mathcal{G}_0}$ is entirely specified by the causal association fields $\{A_j\}_{1\le j\le J}$. The following theorem characterizes the support of these grouplets and Theorem 2.4 proves that this family defines a tight frame.

Theorem 2.3. *For any $m \in \mathcal{G}_0$, $g_{j,m}[n]$ has 1 vanishing moment. If the causal association fields are strictly multiscale then*

- *(i) $h_{J,m}[n] = 1/\sqrt{s[m]}$ over its support whose size is $s[m]$. Support points are before m at a distance strictly smaller than 2^J.*
- *(ii) $g_{j,m}[n]$ takes a constant positive value on support points before n and a constant negative value on support points after n. The distance between m and all support points is smaller than 2^{j-1}.*

Proof. If for any $n \in \mathcal{G}_0$, $f[n] = c$ then one can derive from (21) and (23) that $a[m] = c$ for all $m \in \mathcal{G}_0$. It results from (22) that for all m and j, $d_j[m] = 0$ and hence that $g_{j,m}$ has 1 vanishing moment.

Let us now suppose that the causal association field is strictly multiscale, which means that if $A_j[\tilde{m}] = m$ then $d(m, \tilde{m}) = 2^{j-1}$. After applying k grouping operators, each $a[m]$ is the result of a linear operator applied to $f[n]$ and hence can be written $a[m] = \langle \tilde{h}_{k,m}, f\rangle$. Let $m = \tilde{m} + A_j[\tilde{m}] \in \mathcal{G}_{j+1}$ be the point grouped with $\tilde{m} \in \tilde{\mathcal{G}}_{j+1}$ by the $k+1$ unitary operator. As a result of (23) we have

$$\tilde{h}_{k+1,m}[n] = \frac{s[m]\,\tilde{h}_{k,m}[n] + s[\tilde{m}]\,\tilde{h}_{k,\tilde{m}}[n]}{s[m] + s[\tilde{m}]}. \tag{25}$$

Let us first prove that the supports of $\tilde{h}_{k,m}[n]$ and $\tilde{h}_{k,\tilde{m}}[n]$ do not intersect. Each $\tilde{h}_{k,m}$ has a tree structure rooted at m because of the causality of the association field. Indeed each point of its support is related by the causal association field that groups each point to a unique parent that is *before*. The root m is thus before all other support points. Since the association field is strictly multiscale, The maximum distance between a support point and m is bounded by adding distance between consecutive points that are grouped. At a scale $2^l \leq j$ the distance is 2^{l-1} because the association field is strictly multiscale, and the maximum distance is thus smaller than $\sum_{l=1}^{j} 2^{l-1} < 2^j$.

When grouping a grouplet at $\tilde{m}$ with a grouplet at m, we show that the corresponding trees of $\tilde{h}_{k,m}$ and $\tilde{h}_{k,\tilde{m}}$ are disjoint by proving that m and $\tilde{m}$ do not belong respectively to the support of $\tilde{h}_{k,\tilde{m}}$ and $\tilde{h}_{k,m}$. Clearly m cannot belong to the tree support of $\tilde{h}_{k,\tilde{m}}$ rooted at $\tilde{m}$ because m is before $\tilde{m}$. To prove that $\tilde{m}$ does not belong to the support of $\tilde{h}_{k,m}$, observe that $d(m,\tilde{m}) = 2^{j-1}$ and that all points in the support of $\tilde{h}_{k,m}[n]$ is at a distance of m strictly smaller than 2^{j-1}.

Since the supports of $\tilde{h}_{k,m}$ and $\tilde{h}_{k,\tilde{m}}$ are trees and none of their roots belong to the other tree, necessarily these trees are disjoint which means that these supports do not intersect.

By induction on k, as in the proof of Theorem 2.1, we prove that $h_{J,m}[n] = 1/\sqrt{s[m]}$ over its support whose size is $s[m]$. We already verified that at a scale 2^J support points are *before* m at a distance strictly smaller than 2^J.

To prove (ii), since $d_j[\tilde{m}] = \langle g_{j,\tilde{m}}, f \rangle$, as a result of (22) we can write

$$g_{j,\tilde{m}} = (\tilde{h}_{k,\tilde{m}} - \tilde{h}_{k,m}) \frac{\sqrt{s[m]s[\tilde{m}]}}{\sqrt{s[m] + s[\tilde{m}]}} \ . \tag{26}$$

Since $\tilde{h}_{k,\tilde{m}} = 1/s[\tilde{m}]$ and $\tilde{h}_{k,m} = 1/s[m]$ over their support of size respectively $s[\tilde{m}]$ and $s[m]$, and their support are disjoint, it results that $g_{j,\tilde{m}}$ takes only two different values over its support. Since m is before $\tilde{m}$ and $d(\tilde{m},m) = 2^{j-1}$, using (26) and the support properties of $\tilde{h}_{k,\tilde{m}}$ and $\tilde{h}_{k,m}$ we derive (ii). □

Inverse Grouplet Tight Frame Transform An inverse grouplet frame recovers a signal f from its grouplet coefficients $\{d_j[m] \ , \ a_J[m]\}_{m \in \mathcal{G}_0, 1 \leq j \leq J}$ and the association fields $\{A_j[m]\}_{m \in \mathcal{G}_0}$. Since the representation is redundant, the grouplet transform has an infinite number of left inverses. For noise removal by thresholding, the best inverse is the pseudo-inverse that implements a dual frame reconstruction. We describe a left-inverse that is then proved to be the pseudo-inverse.

The support-size array is recalculated at the coarsest scale 2^J from the association fields. It is initialized to $s[m] = 1$ for all $m \in \mathcal{G}_0$ and for j going from 1 to J and for all $\tilde{m} \in \mathcal{G}_0$

$$m = \tilde{m} + A_j[\tilde{m}], \quad \widehat{s} = s[m] + s[\tilde{m}] \quad \text{and} \quad s[m] = \widehat{s}.$$

The average coefficient normalization (24) is then inverted

$$\forall m \in \mathcal{G}_0 \quad , \quad a[m] = \frac{a_J[m]}{\sqrt{s[m]}} \ . \tag{27}$$

Each grouping operator is then inverted in the reverse order it was calculated. For j decreasing from J to 1 and for n going from N to 1, let $\tilde{m} = \alpha(n)$. The scale support is updated

$$\tilde{s} = s[m] - s[\tilde{m}] \tag{28}$$

If $A_j[\tilde{m}] = \text{NULL}$ then $a[\tilde{m}]$ is not modified. Otherwise, let $m = \tilde{m} + A_j[\tilde{m}]$. The finer scale average coefficients are computed by inverting the grouping transform (22) and (23). A causal reconstruction recovers the average value at $\tilde{m}$ from a coefficient located before :

$$\tilde{a}_- = a[m] + d_j[\tilde{m}] \frac{\sqrt{\tilde{s}}}{\sqrt{s[\tilde{m}]\, s[m]}} \ . \tag{29}$$

An anti-causal reconstruction recovers the average value at m from a coefficient located after :

$$\tilde{a}_+ = a[m] - d_j[\tilde{m}] \frac{\sqrt{s[\tilde{m}]}}{\sqrt{\tilde{s}\, s[m]}} \ , \tag{30}$$

A left inverse averages causal and anti-causal reconstructions. The anti-causal reconstruction is stored in place at m $a[m] = \tilde{a}_+$ and the causal reconstruction at $\tilde{m}$ is averaged with the previously stored anti-causal reconstruction. Theorem 2.4 proves that the pseudo-inverse is implemented with equal averaging weights on causal and anticausal reconstructions :

$$\tilde{a} = \frac{\tilde{a}_- + a[\tilde{m}]}{2} \quad \text{and} \quad a[\tilde{m}] = \tilde{a} \ . \tag{31}$$

The averaging size is then updated $s[m] = \tilde{s}$.

At the end of the loop over all j and n, this left inverse reconstructs $a[m] = f[m]$ for all $m \in \mathcal{G}_0$. If f has N samples, this reconstruction is performed with $O(J\,N)$ operations. Theorem 2.4 proves that this left inverse is the pseudo inverse of the grouplet tight frame transform.

Theorem 2.4. *For any causal multiscale association fields*

$$\forall f \in \mathbf{l^2}(\mathcal{G}_0) \quad , \quad \|f\|^2 = \sum_{j=1}^{J} \frac{1}{2^j} \sum_{m \in \mathcal{G}_0} |\langle f, g_{j,m} \rangle|^2 + \frac{1}{2^J} \sum_{m \in \mathcal{G}_0} |\langle f, h_{J,m} \rangle|^2 \tag{32}$$

so $\{g_{j,m}\ ,\ h_{J,m}\}_{1 \le j \le J, m \in \mathcal{G}_0}$ *is a tight frame of* $\mathbf{l^2}(\mathcal{G}_0)$.
The left inverse with equal averaging weigths on causal and anti-causal reconstructions in (31) is the pseudo-inverse.

Proof. Let $a_j[m] = a[m]\sqrt{s[m]}$ be the normalized average array at the end of the loop over the index n that goes from 1 to N, for a given j. We first prove the following Lemma.

Lemma 2.2. *For any $j > 1$*

$$2\sum_{m\in\mathcal{G}_0} |a_{j-1}[m]|^2 = \sum_{m\in\mathcal{G}_0} |a_j[m]|^2 + \sum_{m\in\mathcal{G}_0} |d_j[m]|^2. \tag{33}$$

To prove this lemma, observe that the grouplet operator can be decomposed as a product of isometric operators. At a fixed scale 2^j, the grouplet transform begins with a duplication operator that transforms $a_{j-1}[m]$ into a pair of signals

$$(a[m]\sqrt{s[m]} = a_{j-1}[m]\ ,\ d[\tilde{m}] = a_{j-1}[\tilde{m}]) \quad \text{for all } m, \tilde{m} \in \mathcal{G}_0.$$

Then the grouplet iteration over n from 1 to N transforms $\{a[m]\sqrt{s[m]}\,,\, d[\tilde{m}]\}_{m,\tilde{m}\in\mathcal{G}_0}$ with a cascade of unitary operators. For each n, if $A[\tilde{m}] = \text{NULL}$ then the operator is the identity. If $A[\tilde{m}] \neq \text{NULL}$ then Lemma 2.1 proves that the operator which transforms $(a[m]\sqrt{s[m]}\,, d[\tilde{m}] = a[\tilde{m}]\sqrt{s[\tilde{m}]})$ into $(\widehat{a}\sqrt{\widehat{s}}, d[\tilde{m}] = d_j[\tilde{m}])$ as defined by (21), (22) and (23) is indeed a unitary operator. It results that $\{a[m]\sqrt{s[m]}, d[\tilde{m}]\}_{m,\tilde{m}\in\mathcal{G}_0}$ is transformed from its initial values $\{a_{j-1}[m], a_{j-1}[\tilde{m}]\}_{m,\tilde{m}\in\mathcal{G}_0}$ into the final values $\{a_j[m], d_j[\tilde{m}]\}_{m\in\mathcal{G}_0,\tilde{m}\in\mathcal{G}_0}$ by a cascade of unitary operators, which is therefore a unitary operator. It implies that norm of these pairs of signals is conserved which proves (33).

Since $a_0[n] = f[n]$, $\langle f, g_{j,m}\rangle = d_j[m]$ and $\langle f, h_{J,m}\rangle = a_J[m]$, the theorem energy conservation (32) is proved with a substitution on (33) for j going from 1 to J.

The grouplet transform is obtained with a loop over operators at increasing scales 2^j. A left inverse is obtained with a product of the left inverse of each elementary operator in the reverse order. The pseudo inverse is the product of the pseudo-inverses of each elementary operator. We saw that at each scale 2^j the grouplet transform begins with a duplication operator followed by a cascade of unitary operators. The inverse of each unitary operator is also unitary and is therefore the pseudo inverse. The duplication operator transforms an array $x[m]$ into a pair $(x[m], x[m])$ for all $m \in \mathcal{G}_0$. Its pseudo-inverse is the averaging that transforms a pair of arrays $(x[m], y[m])$ into $(x[m] + y[m])/2$ for all $m \in \mathcal{G}_0$. For each j, the inverse grouplet algorithm is equivalent to this cascade of inverse unitary operators followed by this averaging. Instead of computing the averaging at the end of the loop over n as in the proof, the reconstruction algorithm computes immediately the averaging (31) for each pair of coefficients. The result is the same because the coefficient $a[\tilde{m}]$ will not be modified anymore by the continuing cascade of inverse operators, which is guaranteed by the causality of the association fields. The averaging is computed immediately because it requires less memory storage. □

General frame theory [18] proves that the pseudo-inverse implements a reconstruction within the dual frame. Theorem 2.4 proves that grouplets define a tight frame and hence that the dual frame is equal to the original frame. The pseudo-inverse algorithm thus computes

$$f[n] = \sum_{j=1}^{J} \frac{1}{2^j} \sum_{m \in \mathcal{G}_0} d_j[m]\, g_{j,m}[n] + \frac{1}{2^J} \sum_{m \in \mathcal{G}_0} a_J[m]\, h_{J,m}[n] \ . \tag{34}$$

2.3 Noise Removal and Image Zooming

A signal contaminated $f[n]$ by a Gaussian white noise $W[n]$ can be estimated by thresholding the coefficients of $X[n] = f[n] + W[n]$ in an orthogonal basis or in a frame. With grouplets, this amounts to a conditional averaging of signal coefficients which have been grouped by the multiscale association fields. Image zooming by geometric interpolation and regularization is a second application that is described. Missing pixels are estimated with adaptive interpolation in directions in which the image is regular.

Orthogonal Grouplets The efficiency of denoising with a thresholding estimator in a basis depends upon the sparsity of the signal within the basis. Grouplets define orthogonal bases and the optimization of the association fields amounts to finding a "best" basis. Ideally one would like to find the "best" basis in which the estimation by thresholding produces a minimum risk. Estimating such a best basis is beyond the scope of this paper but is studied for video denoising in [19].

The grouplet denoising approach described in the following gives numerical illustrations of grouplet properties, with no optimality result. The association field is computed on the noisy image $X[n]$ with the block matching optimization (17). For a Gaussian white noise $W[n]$ of variance σ^2, the blocks are square windows of width proportional to σ so that the averaging regularization compensates the noise variance. The orthogonal grouplet coefficients of $X[n]$ below a threshold T are set to zero and a signal estimate $\widehat{F}[n]$ is reconstructed :

$$\hat{F}[n] = \sum_{j=1}^{J} \sum_{\tilde{m} \in \mathcal{G}_j} \rho_T(\langle X, g_{j,\tilde{m}} \rangle)\, g_{j,\tilde{m}}[n] + \sum_{m \in \mathcal{G}_J} \rho_T(\langle X, h_{J,m} \rangle)\, h_{J,m}[n], \tag{35}$$

with $\rho_T(x) = 0$ if $|x| < T$ and $\rho_T(x) = x$ otherwise. In our numerical experiments $T = \mu\, \sigma$ with $\mu = 3$.

Fig. 7(b) shows a noisy seismic image contaminated by an additive Gaussian white noise. The PSNR is 26db. Fig. 7(c) shows the resulting grouplet coefficients calculated from the multiscale association fields obtained with block matchings.

Fig. 7(d) shows the coefficients above threshold and the reconstructed seismic image in Fig. 7(e) has a PSNR of 27.3db. Setting a coefficient to zero is equivalent to average the image over the corresponding grouplet support. This grouplet thresholding thus performs an adaptive multiscale averaging of the signal along the directions of the multiscale association fields. The reconstructed signal has less noise but the discontinuities of the grouplets create blocking artifacts that appear in Fig. 7(e).

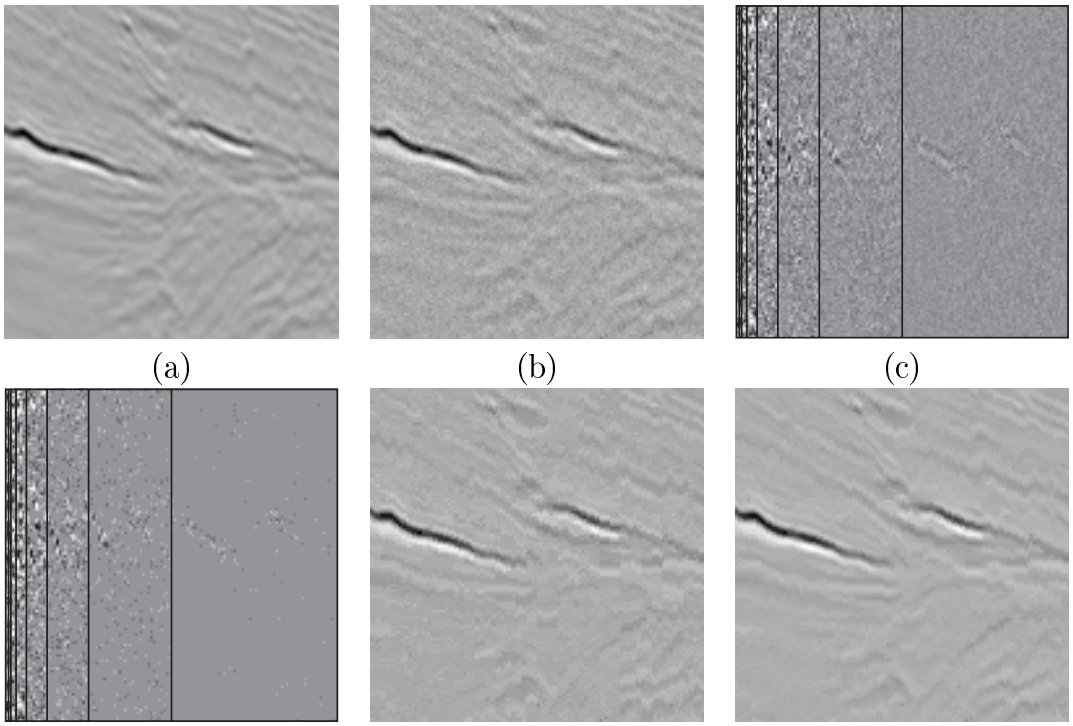

FIG. 7 – *(a) : Original image. (b) : Noisy seismic image (PSNR = 26db). (c) : Orthogonal noisy grouplet coefficients. (d) : Thresholded noisy grouplet coefficients. (e) : Image reconstructed from thresholded orthogonal grouplet coefficients (PSNR = 27.3db). (f) : Image reconstructed from thresholded tight frame grouplet coefficients (PSNR = 29.5db).*

Grouplets Tight Frames Denoising by thresholding on a grouplet tight frame improves the estimation. The denoising estimator thresholds the frame grouplet coefficients and reconstructs a signal with a left inverse. To minimize the expected risk with a Gaussian white noise, it is necessary to use the pseudo-inverse, in which

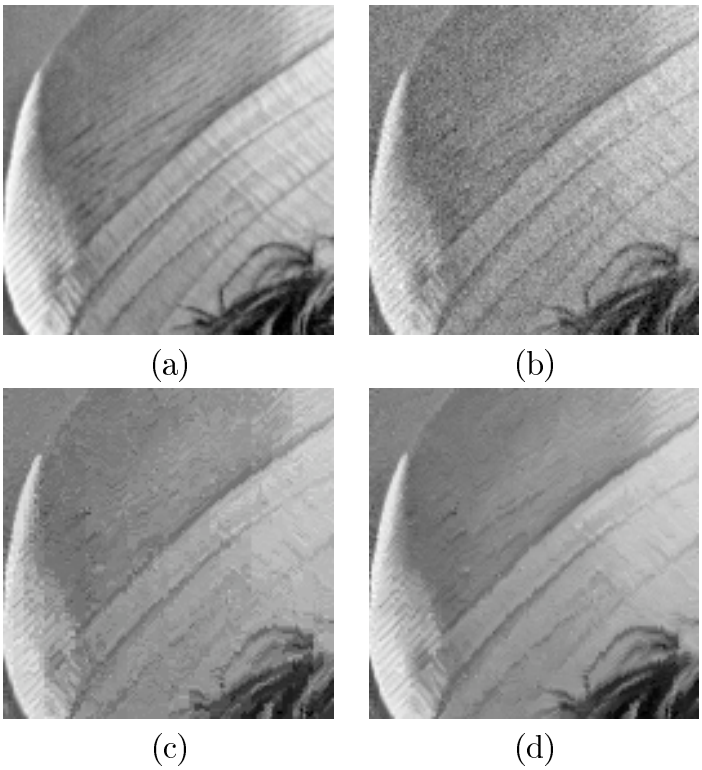

FIG. 8 – *(a) : Lena hat. (b) : Noisy image (PSNR = 27.8db). (c) : Orthogonal grouplet denoising (PSNR = 28.7db). (d) : Tight frame grouplet denoising (PSNR = 30.9db).*

case the estimator is defined by

$$\widehat{F}[n] = \sum_{j=1}^{J} \frac{1}{2^j} \sum_{m \in \mathcal{G}_0} \rho_T(\langle X, g_{j,m} \rangle)\, g_{j,m}[n] + \frac{1}{2^J} \sum_{m \in \mathcal{G}_0} \rho_T(\langle X, h_{J,m} \rangle)\, h_{J,m}[n]. \qquad (36)$$

With a pseudo-inverse, a tight frame thresholding is similar to averaging thresholding estimators in several orthonormal bases, which explains why it reduces the risk compared to a thresholding estimator in a single basis.

A multiscale association field is calculated from the noisy seismic image in Fig. 7(b) with a block matching algorithm. The resulting grouplet tight frame coefficients are also thresholded with $T = 3\,\sigma$. Fig. 7(f) shows the resulting estimation obtained by applying an inverse grouplet transform with a PSNR of $29.5db$. As expected, the risk is much smaller than with a grouplet orthogonal basis and the blocking artifacts produced by the orthogonal basis are reduced in the tight frame estimation. Fig. 8 gives another example of image denoising on a grey-level image. Grouplet tight frame denoising yields again a PSNR that is $2db$ above an orthogo-

nal grouplet denoising. Although the tight frame redundancy reduces the artifacts, the reconstructed image still has irregularities due to the grouplet non-regularity. This motivates applying a grouplet transform not on the image but on a wavelet transform of the image, to inherit the regularity of wavelets as explained by Section 3.

When computing the association field with a block matching, a grouplet tight frame denoising has similarities with a non local mean denoising algorithm [2]. A non local mean denoising averages a noisy signal sample with other non local "neighbors" defined as image points having a block neighborhood which is sufficiently close to the block neighborhood of the original noisy signal sample. Thresholding a grouplet transform performs a similar averaging since points are also grouped, potentially with a block matching, however the grouping is performed with multiscale procedure and the averaging decision depends upon a different thresholding criteria that involves a normalized inner product.

Image Zooming Image zooming requires to compute intermediate pixels to enlarge the image size. Images are most often sampled at a sampling rate that is below the Nyquist rate. Since the sampling density is not sufficient, missing samples cannot be computed with a linear interpolation operator. However, in presence of anisotropic geometric regularity one can compute precise approximations of missing samples by interpolating the image in the direction in which it is regular. Many algorithms have been developed to implement such directional interpolations, including variational approaches [21]. The following zooming algorithm performs directional interpolations and regularizations according to a multiscale association field with a thresholding in a grouplet frame.

For zooming, signal values are computed on a larger grid for all $m \in \mathcal{G}_0$ knowing noisy values $X[n] = f[n] + W[n]$ on a subgrid $n \in \widehat{\mathcal{G}}_0$. At each scale 2^j, to compute an association field $A_j[m]$ on the full grid $\mathcal{G}_0$, missing samples $X[m]$ for $m \in \mathcal{G}_0 - \widehat{\mathcal{G}}_0$ are estimated with a standard linear interpolation operator. This interpolation is not precise because of the aliasing, and the interpolation error can be interpreted as another source of noise. The multiscale association field is calculated from these interpolated noisy data with a block matching over sufficiently large blocks to be nearly insensitive to the noise. The tight frame grouplet transform is also modified to take into account missing samples. The zooming and denoising algorithm described below decompose the noisy image in a grouplet tight frame using a multiscale association field defined over the full grid $\mathcal{G}_0$. The resulting grouplet coefficients are thresholded and an inverse transform over the full grid $\mathcal{G}_0$ restores a higher resolution signal over $\mathcal{G}_0$.

The averaging size array is initialized to take into account missing data. We set $s[m] = 1$ if $m \in \widehat{\mathcal{G}}_0$. For missing samples $m \in \mathcal{G}_0 - \widehat{\mathcal{G}}_0$, we set $s[m] = 0$ and

$X[m] = \text{NULL}$.

Let N be the total number of samples in $\mathcal{G}_0$ and 2^J be the maximum scale. For j going from 1 to J and for n going from 1 to N, let $\tilde{m} = \alpha(n)$. The grouplet computation is identical to the previously described tight frame transform computation when the association field groups existing sample points. When the grouping includes a missing sample, the calculation is modified accordingly. If $A_j[\tilde{m}] = \text{NULL}$ then $d_j[\tilde{m}] = a[\tilde{m}]\sqrt{s[\tilde{m}]}$. If $A_j[\tilde{m}] \neq \text{NULL}$ let $m = \tilde{m} + A_j[\tilde{m}]$. If $s[\tilde{m}] = 0$, which we means that it is a missing point, then we set $d_j[\tilde{m}] = 0$. If $s[\tilde{m}] \neq 0$ then as in (22) and (23), we set $\widehat{s} = s[m] + s[\tilde{m}]$,

$$d_j[\tilde{m}] = (a[m] - a[\tilde{m}])\frac{\sqrt{s[m]s[\tilde{m}]}}{\sqrt{\widehat{s}}} \quad \text{and} \quad \widehat{a} = \frac{s[m]\,a[m] + s[\tilde{m}]\,a[\tilde{m}]}{\widehat{s}}.$$

These values are stored "in place" : $a[m] = \widehat{a}$ and $s[m] = \widehat{s}$.

At the coarsest scale 2^J, the average coefficients are also normalized

$$\forall m \in \mathcal{G}_0 \quad , \quad a_J[m] = a[m]\,\sqrt{s[m]}\;. \tag{37}$$

A zooming process includes a denoising step implemented by a thresholding that sets to zero all grouplet coefficients below a threshold T .

The inverse tight frame transform performs an averaging of associated points when the corresponding grouplet coefficient is equal to zero. This transform is modified to compute values for missing samples. There are two reasons why a difference grouplet coefficient $d_j[m]$ may be zero. Either it was set to zero by a thresholding or it was originally zero because the data was missing. In both case, an averaging is calculated. This amounts to compute missing values by averaging them in the direction of the multiscale association flow, while regularizing these averages with the grouplet thresholding.

The inverse grouplet transform is essentially the same as the pseudo-inverse, while taking into account potentially missing data. The support-size array is recalculated at the coarsest scale 2^J. At the finest scale $s[m] = 1$ if $m \in \widehat{\mathcal{G}}_0$ and $s[m] = 0$ if $m \in \mathcal{G}_0 - \widehat{\mathcal{G}}_0$. Then for j going from 1 to J and for all $\tilde{m} \in \mathcal{G}_0$ and $m = \tilde{m} + A_j[\tilde{m}]$, we set $\widehat{s} = s[m] + s[\tilde{m}]$ and $s[m] = \widehat{s}$. The normalization (37) is then inverted : $a[m] = a_J[m]/\sqrt{s[m]}$ for $m \in \mathcal{G}_0$. Each grouping operation is then inverted for j going from J to 1. For n going from N to 1 and $\tilde{m} = \alpha(n)$, if $A_j[\tilde{m}] \neq \text{NULL}$ let $m = \tilde{m} + A_j[\tilde{m}]$ and

$$\tilde{s} = s[m] - s[\tilde{m}]. \tag{38}$$

If $s[\tilde{m}] = 0$ and $a[\tilde{m}] = \text{NULL}$ then we set $a[\tilde{m}] = a[m]$. If $s[\tilde{m}] = 0$ and $a[\tilde{m}] \neq \text{NULL}$ and $\widehat{s} \neq 0$ then we set $\widehat{a} = (a[\tilde{m}] + a[m])/2$ and $a[\tilde{m}] = \widehat{a}$. If $s[\tilde{m}] \neq 0$ and

$\widehat{s} = 0$ then $s[m] = 0$. Otherwise if $s[\tilde{m}] \neq 0$ and $\widehat{s} \neq 0$ then

$$\tilde{a}_1 = a[m] - d_j[\tilde{m}] \frac{\sqrt{s[\tilde{m}]}}{\sqrt{\tilde{s}\, s[m]}} \tag{39}$$

$$\tilde{a}_2 = a[m] + d_j[\tilde{m}] \frac{\sqrt{\tilde{s}}}{\sqrt{s[\tilde{m}]\, s[m]}} \ . \tag{40}$$

The first average is stored "in place", $a[m] = \tilde{a}_1$ and $s[m] = \tilde{s}$. The second reconstructed average is calculated as in (31)

$$a[m] = \bar{a}_2 \quad \text{with} \quad \bar{a}_2 = \frac{a[\tilde{m}] + \tilde{a}_2}{2} \ .$$

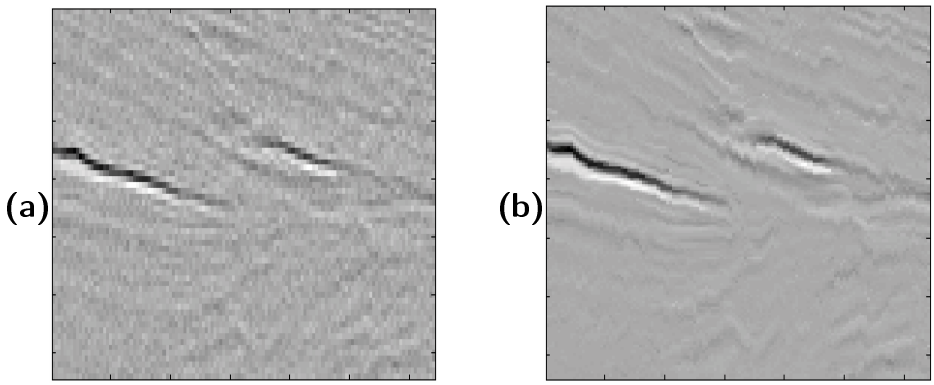

FIG. 9 – *(a) : Subsampled noisy seismic image. (b) : Regularized zoom, with twice more columns, computed by thresholding tight frame grouplet coefficients.*

Fig. 9(b) shows an example of zooming calculated from an aliased seismic noisy image in Fig. 9(a). The zoom increases the number of columns by a factor 2. Both images are shown at the same size. Despite the presence of noise, the regularization and direction interpolation performed by the grouplet thresholding restores in Fig. 9(b) geometric structures that are barely visible in Fig. 9(a).

3 Grouping Bandlets

Instead of applying a grouplet transform directly on the original image, one may rather apply this transform on a wavelet transform of the image, which already provides a sparse representation. Indeed wavelet coefficients are obtained through a convolution with a dilated wavelet and hence inherit the geometric regularity of the original image. Transforming these wavelet coefficients along directions where

they are geometrically regular can thus further improve the sparsity of wavelet representation. This is the central idea of bandlet constructions. Several approaches have already been proposed to construct bandlet orthonormal bases by applying an orthogonal transform on wavelet coefficients [14, 22]. Applying a grouplet transform over wavelet coefficients is a different approach that yields *grouping bandlet* coefficients. This construction has a hierarchical structure that could be compared to association field models of horizontal connections between V1 simple cells [8]

Section 3.1 begins by defining orthogonal grouping bandlet bases from orthogonal wavelet bases. Section 3.2 introduces tight frame grouping bandlets constructed over steering pyramid wavelets and separable tight frame wavelets. It compares noise removal by thresholding in a bandlet tight frame and in a wavelet tight frame.

3.1 Orthogonal Grouping Bandlet Bases

Orthogonal grouping bandlet bases are constructed by applying an orthogonal grouplet transform on orthogonal wavelet coefficients. Separable orthogonal wavelet bases of $\mathrm{L}^2([0,1]^2)$ are obtained by dilating and translating three separable wavelets $\{\psi^k\}_{1\leq k\leq 3}$ that have vanishing moments. For $x=(x_1,x_2)$ and $n=(n_1,n_2)$, the resulting wavelet basis of $\mathrm{L}^2([0,1]^2)$ can be written

$$\mathcal{B}=\left\{\psi^k_{l,n}(x)=2^{-l}\,\psi^k(2^{-l}x-n)\right\}_{l<0,2^l n\in[0,1]^2,k=1,2,3}, \tag{41}$$

modulo modifications of the wavelet at the boundaries of $[0,1]^2$. Inner products with these translated wavelets can be written as a convolution product

$$W^k_l f[n]=\langle f,\psi^k_{l,n}\rangle = f\star\tilde{\psi}^k_l(2^l n) \quad \text{with} \quad \tilde{\psi}^k_l(x)=2^{-l}\,\psi^k(-2^{-l}x)\ . \tag{42}$$

Each wavelet transform image $Wf^k_l[n]$ is thus obtained by filtering the image with a dilated wavelet $\tilde{\psi}^k_l(x)$, which is a band-pass filter along the vertical direction for $k=1$, along the horizontal direction for $k=2$ and along both directions for $k=3$.

An orthogonal grouplet transform of each wavelet transform image $W^k_l f[n]$ is defined by computing multiscale association fields. For the first direction $k=1$, wavelet coefficients $W^1_l f[n]$ have a large amplitude near sharp vertical variations, which may belong to edges that can be parametrized horizontally. This appears at all scales 2^l in Fig. 10(b). To group wavelet coefficients that are in different columns, the grouplet transform is constructed with column embedded subgrids that correspond to a subsampling of the columns of the wavelet coefficient images $W^1_l f[n]$, as explained in Section 2.1. Multiscale association fields computed over these grids define orthogonal grouplet bases, where the grouplet vectors are elongated across columns and can thus take advantage of geometric regularity across columns. This orthogonal grouplet decomposition is performed for all scales 2^j for $1\leq j\leq J$.

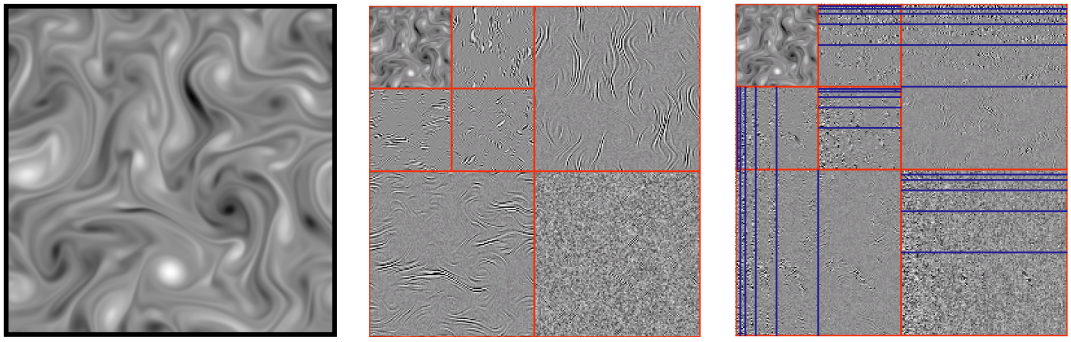

(a) (b) (c)

FIG. 10 – *(a) : Original image. (b) : Orthogonal wavelet coefficients. (c) : Orthogonal grouping bandlet coefficients.*

For the second direction $k = 2$, large wavelet coefficients correspond to sharp transitions horizontally that belong to structures spread across several rows. The orthogonal grouplet transform is thus defined with row embedded subgrids that correspond to a subsampling of the rows of the wavelet coefficient images $W_l^2 f[n]$. The resulting grouplet vectors are elongated vertically across rows.

For the third direction $k = 3$, the wavelets $\tilde{\psi}_j^3$ perform a high pass filtering along vertical and horizontal directions. Large coefficients thus belong to geometric structures that are spread across several rows and columns. A grouplet transform can thus take advantage of this geometric regularity by defining column embedded subgrids or row embedded subgrids. Fig. 10(c) shows grouping bandlet coefficients obtained with grouplet transforms using different multiscale association fields for each wavelet image $W_l^k f[n]$. Bandlet coefficients are displayed with the same dynamic range as the corresponding original wavelet coefficients. The number of large amplitude coefficients is reduced. Although grouplet coefficients are more sparse than wavelet coefficients in Fig. 10, it does not mean that the representation is more efficient for image coding. Indeed, a compression algorithm also needs to encode the multiscale association fields.

The cascade of a wavelet orthonormal transform followed by grouplet transforms defines an orthonormal transform that we call a "bandlet transform". A bandlet orthonormal basis of $\mathbf{L^2}[0,1]^2$ is a family of functions

$$\left\{ b_{l,j,m}^k(x) \right\}_{m \in \tilde{\mathcal{G}}_j, 1 \leq j \leq J, l < 0, 1 \leq k \leq 3}.$$

which is the result of applying a grouplet orthonormal transform on a wavelet orthonormal basis (41). These bandlets can be written

$$b_{l,j,m}^k(x) = \sum_n g_{j,m}^{k,l}[n]\, \psi_{l,n}^k(x) \tag{43}$$

where $\{g^{k,l}_{j,m}[n], h^{k,l}_{J,m}[n]\}_{j,m}$ is the grouplet basis corresponding to the multiscale association fields computed over orthogonal wavelet coefficients for the direction k and scale 2^l.

(a) (b)

FIG. 11 – *(a) : Examples of orthogonal grouplets. (b) : Orthogonal grouping bandlets corresponding to the grouplets in (a).*

Grouplets have no regularity but grouping bandlets in (43) have the same regularity as the wavelets $\psi^k(x)$. The support of $b^k_{l,j,m}(x)$ has a width proportional to 2^l around the grouplet $g^{k.l}_{j,m}$ and a length typically proportional to 2^j. Fig. 11 gives examples of grouplets and the corresponding bandlets.

3.2 Tight Frames of Grouping Bandlets and Denoising

To remove noise in images, thresholding translation invariant wavelet frame coefficients yields better estimators than thresholding orthogonal wavelet coefficients. Grouplet tight frames also yields better estimators by using a more flexible model of association fields than grouplet orthogonal bases. Applying grouplet tight frames to wavelet tight frame defines a tight frame of bandlet functions.

A separable wavelet frame is constructed by oversampling an orthogonal or a biorthogonal wavelet transform. From three separable orthogonal or biorthogonal wavelets $\psi^k(x)$ for $k = 1, 2, 3$, the oversampled is defined by :

$$W f^k_l[n] = f \star \tilde{\psi}^k_l(n) \quad \text{with} \quad \tilde{\psi}^k_l(x) = 2^{-l}\, \psi^k(-2^{-l}x) \quad \text{for } k = 1, 2, 3. \tag{44}$$

Fig. 12 gives an example at scales $2^l = 2^1, 2^2$.

A wavelet thresholding removes a Gaussian white noise of variance σ^2 from a noisy image X by setting to zero all dyadic wavelet coefficient $W^k_l X[n]$ whose amplitude is below a threshold $T = \mu\,\sigma$, and by applying the inverse wavelet transform. In images of 512 by 512 pixels, μ is typically equal to 3. When the image is regular or if the edges or textures are too weak, the thresholding sets all coefficients to zero which averages the noisy coefficients. The two zooms in Fig.

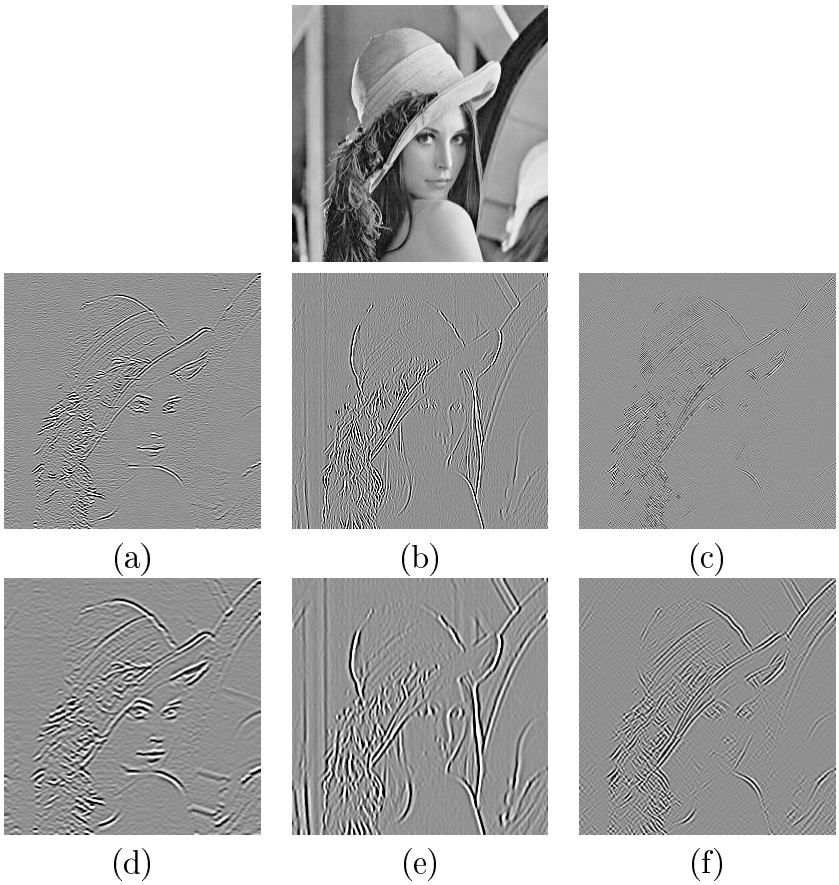

FIG. 12 – *Top : original image. (a,b,c) : dyadic wavelet transform at scale* $2^l = 2$ *along the 3 orientations. (d,e,f) : dyadic wavelet transform at scale* $2^l = 4$.

14 and 15 show that it removes fine textures such as the fine strip hat texture or hairs, while randomly leaving isolated fine structures corresponding to wavelet coefficients above threshold. This wavelet denoising is improved by a grouplet transform over wavelet coefficients, that takes advantage of the geometric regularity of edges and textures.

Grouplet tight frame coefficients are defined from strictly causal multiscale association fields, that relate wavelet coefficients $W_l^k f[n]$ for a fixed direction and scale. These causal association fields are defined with a partial ordering and a pseudo-distance that depends on the preferential direction of the wavelet. For example, if the wavelet is band-pass vertically then it extracts image structures that are rather horizontal. Hence, for $k = 1$, at each scale these association fields are computed with a 0 angle partial ordering (horizontal direction) and a 0 angle partial distance, to obtain horizontal groupings. In this case, at a scale 2^j, the association field groups points from any given column to a point in the column

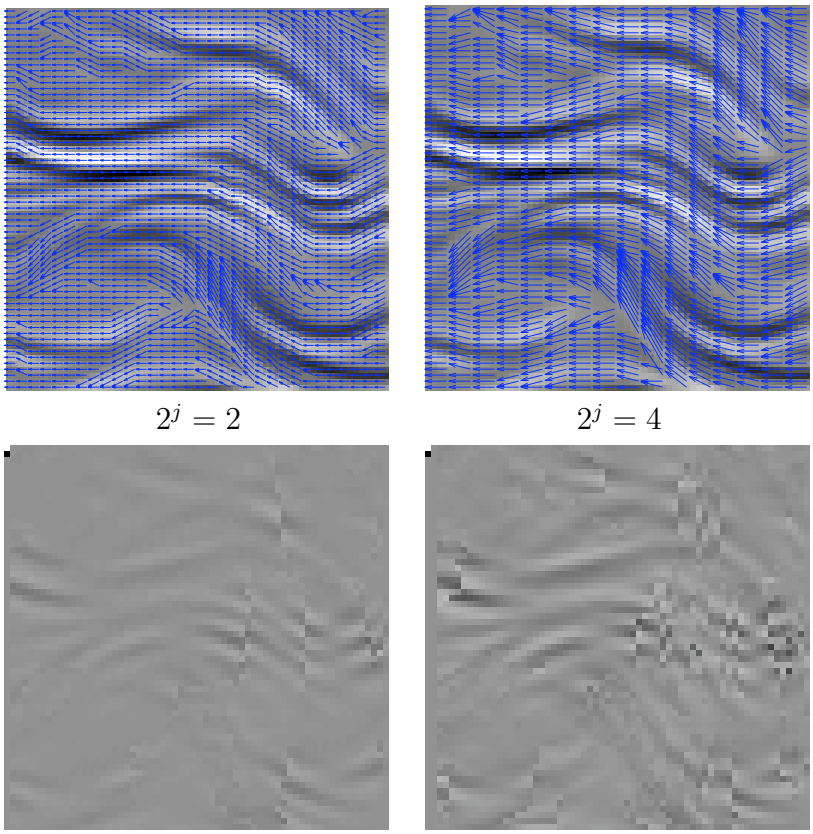

FIG. 13 – *Left and right columns display multiscale causal association fields at different scales 2^j, calculated on wavelet coefficients. The resulting grouping bandlet coefficients are shown below, on the same dynamic range as wavelet coefficients.*

located before at a distance 2^{j-1}. For $k = 2$ which corresponds to wavelets extracting vertical structures, groupings are performed with a $\pi/2$ angle partial ordering (vertical direction), and a $\pi/2$ angle pseudo distance. At a scale 2^j, the grouping is thus performed across rows at a distance 2^{j-1}. For $k = 3$, the groupings can be performed horizontally or vertically. In the numerical computations shown here, groupings are computed horizontally for $k = 3$.

Fig. 13 shows strictly multiscale causal association fields computed on wavelet coefficients at a scale 2^2 in the horizontal orientation, with a block matching. Large amplitude wavelet coefficients correspond to sharp transitions that have a nearly horizontal orientation. The amplitude of the corresponding grouping bandlet coefficients in Fig. 13 is much smaller, because grouplets take advantage of the geometric regularity of wavelet coefficients.

For noise removal, bandlet coefficients below a threshold $T = \mu'\sigma$ with $\mu' = 4$ are set to zero. Observe that μ' is larger than the parameter $\mu = 3$ chosen for wave-

lets, in order to compensate for the partial "noise fitting" that may be produced by the association fields computed on noisy coefficients with a block matching. Fig. 14 and 15 compare the denoising results of a translation invariant wavelet thresholding and of the grouping bandlet tight frame thresholding. Grouping bandlets restore fine textures on Lena's hat or on its hairs because the elongation of these bandlets along these geometrical structures better compresses the signal and yields coefficients above threshold which restore these geometrical structures. On Lena, a grouping bandlet thresholding estimation improves a wavelet thresholding estimation by more than $1db$. However, the multiscale association field must be computed and regularized carefully to avoid creating geometric bandlet artifacts in regular image regions. Optimizing the multiscale association fields to minimize the grouping bandlet estimation risk is an open problem that is beyond the scope of this paper.

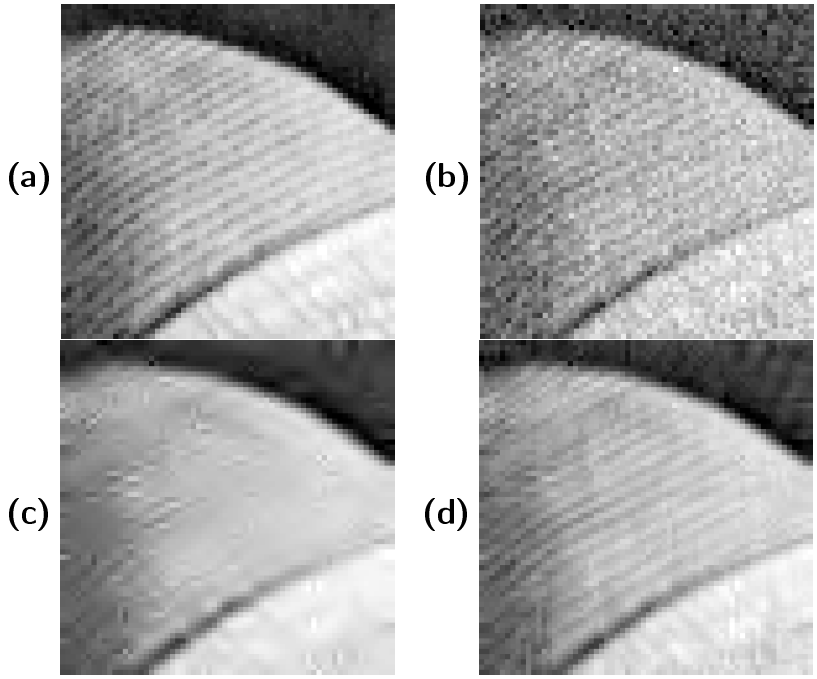

FIG. 14 – *(a) : Original image. (b) : Noisy image. (c) : Translation invariant wavelet thresholding. (d) : Grouping bandlet tight frame thresholding.*

Acknowledgments I would like to thank very much Valérie Charoing for our collaboration and the many discussions we had on this topic, and Gabriel Peyré for his generous help on numerical experiments and figures.

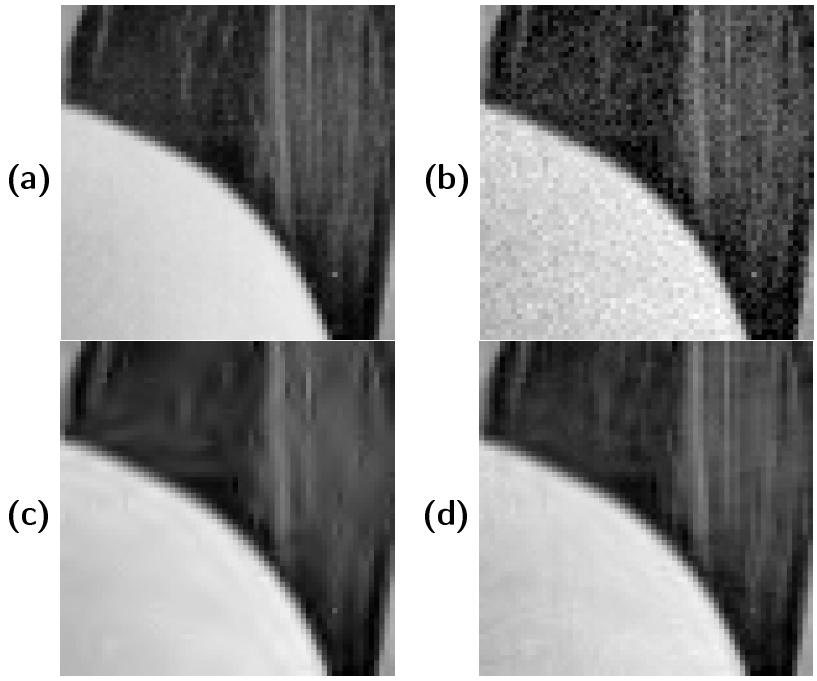

FIG. 15 – *(a) : Original image. (b) : Noisy image. (c) : Translation invariant wavelet thresholding. (d) : Grouping bandlet tight frame thresholding.*

Références

[1] P. C. Bressloff and J. D. Cowan. The functional geometry of local and horizontal connections in a model of v1. *J Physiol Paris*, 97(2-3) :221–236, Mar-May 2003.

[2] A. Buades, B. Coll, and J. M. Morel. A review of image denoising methods, with a new one. *SIAM Multiscale Modeling and Simulation*, 4(2) :490–530, 2005.

[3] E. Candès and D. Donoho. *Curvelets : A surprisingly effective nonadaptive representation of objects with edges*. Vanderbilt University Press, 1999.

[4] C. L. Chang and B. Girod. Direction-adaptive discrete wavelet transform via directional lifting and bandeletization. In *Proc. IEEE International Conference on Image Processing*, October 2006.

[5] V. Chappelier and C. Guillemot. Oriented 1d wavelet transform on a quincunx pyramid for image compression. *Proc. IEEE Int. Conf. on Image Processing*, September 2005.

[6] M. N. Do and M. Vetterli. The contourlet transform : an efficient directional multiresolution image representation. *IEEE Transactions Image on Processing, To appear*, 2005.

[7] D. Donoho. Wedgelets : Nearly-minimax estimation of edges. *Ann. Statist*, 27 :353–382, 1999.

[8] D. J. Field, A. Hayes, and R. F. Hess. Contour integration by the human visual system : evidence for a local "association field". *Vision Research*, 33(2) :173–193, 1993.

[9] Kanizsa G. *Organization in Vision : Essays on Visual Percpetion.* Praeger, 1979.

[10] O. N. Gerek and A. E. Cetin. Adaptive polyphase subband decomposition structures for image compression. *IEEE Trans. on Image Processing*, pages 1649–1660, October 2000.

[11] D J Heeger, E P Simoncelli, and J A Movshon. Computational models of cortical visual processing. *Proc National Academy of Science*, 93 :623–627, 1996.

[12] H. Heijmans, B. Pesquet-Popescu, and G. Piella. Building nonredundant adaptive wavelets by update lifting. *Applied Computational Harmonic Analysis*, (18) :252–281, May 2005.

[13] R. F. Hess, A. Hayes, and D. J. Field. Contour integration and cortical processing. *J Physiol Paris*, 97(2-3) :105–119, Mar-May 2003.

[14] E. Le Pennec and S. Mallat. Sparse Geometrical Image Approximation with Bandelets. *IEEE Transaction on Image Processing*, 14(4) :423–438, 2004.

[15] E. Le Pennec and S. Mallat. Bandelet Image Approximation and Compression. *SIAM Multiscale Modeling and Simulation*, 4(3) :992–1039, 2005.

[16] Tai Sing Lee. Computations in the early visual cortex. *J Physiol Paris*, 97(2-3) :121–139, Mar-May 2003.

[17] L. Luo, F. Wu, S. Li, and Z. Zhuang. Advanced lifiting-based motion-threading technique for the 3d wavelet video coding. *Proceedings of the SPIE*, 5150, 2003.

[18] S. Mallat. *A Wavelet Tour of Signal Processing.* Academic Press, San Diego, 1999.

[19] S. Mallat and G. Yu. Video denoising with grouping bandlets. In *Technical Report 2008 : CMAP, Ecole Polytechnique*, 2008.

[20] S. Mallat and Z. Zhang. Matching pursuits with time-frequency dictionaries. *IEEE Transactions on Signal Processing*, 41(12) :3397–3415, 1993.

[21] S. Masnou. Disocclusion : a variational approach using level lines. *IEEE Trans. On Image Processing*, 11(2) :68–76, 2002.

[22] G. Peyré and S. Mallat. Surface compression with geometric bandelets. *ACM Transactions on Graphics, (SIGGRAPH'05)*, 24(3), Aug. 2005.

[23] A. Secker and D. Taubman. Lifting-based invertible motion adaptive transform (limat) framework for highly scalable video compression. *IEEE Transactions on Image Processing*, 12(12) :1530–1542, December 2003.

[24] D. V. Ville, T. Blu, and M. Unser. On the multidimensional extension of the quincunx subsampling matrix. *IEEE Signal Processing Letters*, 12(2) :112–115.

[25] Bosking W, Zhang Y., Schoenfield B., and Fitzpatrick D. Orientation selectivity and the arrangement of horizontal connections in tree shrew striate cortex. *Journal of Neuroscience*, 17(6) :2112–2127, 1997.